Diindeno-fusion of an anthracene as a design strategy for stable organic biradicals

Gabriel E. Rudebusch[1], José L. Zafra[2], Kjell Jorner[3], Kotaro Fukuda[4], Jonathan L. Marshall[1], Iratxe Arrechea-Marcos[2], Guzmán L. Espejo[2], Rocío Ponce Ortiz[2], Carlos J. Gómez-García[5], Lev N. Zakharov[6], Masayoshi Nakano[4*], Henrik Ottosson[3*], Juan Casado[2*] and Michael M. Haley[1*]

[1]Department of Chemistry & Biochemistry and the Materials Science Institute, University of Oregon, Eugene, Oregon 97403-1253, USA. [2]Department of Physical Chemistry, University of Malaga, Campus de Teatinos s/n 229071 Malaga, Spain. [3]Department of Chemistry – BMC, Uppsala University, Box 576, 751 23 Uppsala, Sweden. [4]Department of Materials Engineering Science, Graduate School of Engineering Science, Osaka University, Toyonaka, Osaka 560-8531, Japan. [5]Instituto de Ciencia Molecular, Universidad de Valencia 46980 Paterna, Valencia, Spain. [6]CAMCOR, University of Oregon, Eugene, Oregon 97403-1433, USA.

haley@uoregon.edu; casado@uma.es; mnaka@cheng.es.osaka-u.ac.jp; henrik.ottosson@kemi.uu.se

Table of Contents

1. Synthesis

1.1 General procedures

All reactions were carried out under nitrogen atmosphere using standard Schlenk line techniques. Toluene was refluxed with sodium for 2 days before distillation and use. Tetrahydrofuran was refluxed with sodium/benzophenone ketyl for 24 hours prior to distillation and use. Boron trifluoride diethyl etherate was distilled from calcium hydride. DDQ was recrystallized from chloroform. All other reagents were used as received. Compound **1** was prepared according to the literature procedure.[1] ^{1}H and ^{13}C NMR spectra were recorded using a Varian Inova 500 (^{1}H: 500.11 MHz, ^{13}C: 125.75 MHz) or Bruker Avance-III-HD 600 (^{1}H: 599.98 MHz, ^{13}C: 150.87 MHz) NMR spectrometer. Chemical shifts (δ) are expressed in ppm relative to the residual protio-solvent. UV-Vis spectra were recorded on a HP 8453 UV-Vis spectrometer. High resolution mass spectra were recorded on a JEOL MS-Route mass spectrometer.

1.2 Synthesis of Compound 2
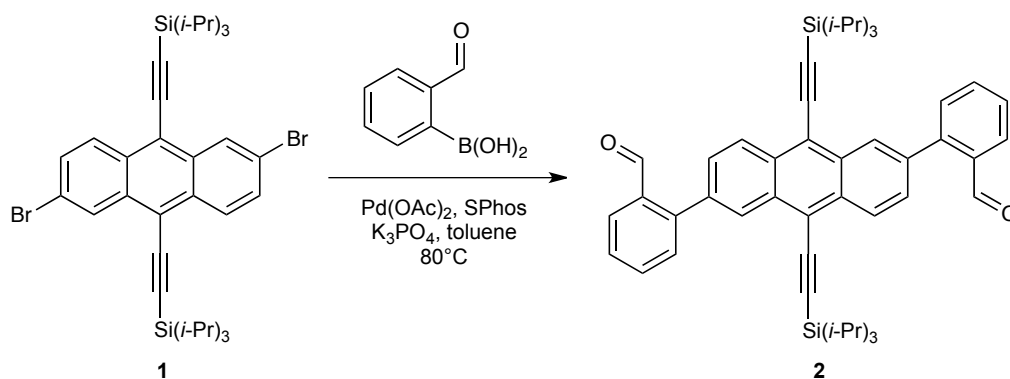
To a 100 ml unregulated pressure vessel equipped with a magnetic stir bar was added compound **1** (1.50 g, 2.15 mmol, 1.00 equiv.), 2-formylbenzeneboronic acid (0.81 g, 5.38 mmol, 2.50 equiv.), K_3PO_4 (1.25 g, 6.5 mmol, 3.00 equiv.) and toluene (25 ml). The mixture was sparged with N_2 for twenty minutes then palladium(II) diacetate (10 mg, 0.043 mmol, 2 mol%) and SPhos (35 mg, 0.086 mmol, 4 mol%) were added and the mixture was sparged with N_2 for ten minutes. The vessel was sealed with a PTFE cap and stirred at 80 °C for 18 h. Upon cooling to room temperature, the reaction mixture was diluted with diethyl ether (50 ml) and washed with water (100 ml) then brine (100 ml). The organic phase was dried over anhydrous magnesium sulfate and filtered. Removal of volatiles under reduced pressure afforded **2** as an orange solid

(1.60 g, >95%); melting point (m.p.), 226-227 °C; ^{1}H NMR (500 MHz, CDCl$_3$, 25 °C), δ (ppm) 10.18 (d, J = 0.8 Hz, 2H), 8.77 – 8.72 (m, 4H), 8.15 (dd, J = 7.9, 1.4 Hz, 2H), 7.77 – 7.70 (m, 4H), 7.67 (dd, J = 7.7, 1.2 Hz, 2H), 7.61 (t, J = 7.7 Hz, 2H), 1.24 (br s, 42H); ^{13}C NMR (126 MHz, CDCl$_3$, 25 °C), δ (ppm) 191.94, 145.38, 136.61, 133.83, 133.62, 132.36, 131.98, 131.06, 129.44, 128.77, 128.20, 128.03, 127.56, 119.19, 106.27, 102.68, 18.87, 11.45; high-resolution mass spectroscopy (HRMS) (ES+) (m/z), calculated for C$_{50}$H$_{59}$O$_2$Si$_2$ (M+H)$^+$ 747.4048, found 747.4034; elemental analysis (EA) calculated for C$_{50}$H$_{58}$O$_2$Si$_2$ C 80.37%, H 7.82%, found C 80.38%, H 7.78%.

1.3 Synthesis of Compound 3
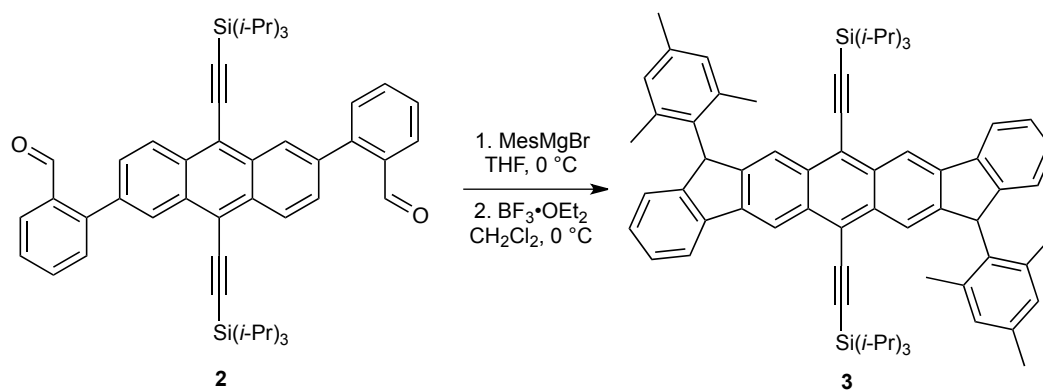
An oven-dried 100 ml flask equipped with a stir bar was charged with **2** (1.00 g, 1.34 mmol) and dry tetrahydrofuran (THF, 50 ml). The flask was cooled to 0 °C then a THF solution of 2-mesitylmagnesium bromide (1M, 5.4 ml, 4.00 equiv.) was added via syringe. After stirring for one hour, the reaction was quenched with saturated aqueous NH$_4$Cl solution (25 ml) and diluted with diethyl ether (50 ml). The organic phase was dried over anhydrous magnesium sulfate and filtered. Volatiles were removed under reduced pressure. The crude diol was dissolved in dry dichloromethane (150 ml) and cooled to 0 °C. Boron trifluoride diethyl etherate (0.66 ml, 5.4 mmol, 4.00 equiv.) was added dropwise and the dark solution was stirred for five minutes. With vigorous stirring, the excess catalyst was quenched by addition of saturated aqueous NaHCO$_3$ solution (25 ml). The organic phase was concentrated under reduced pressure to 25 ml then ethanol (25 ml) was added. The mixture was filtered and washed with water to provide **3** as a yellow solid (1.01 g, 79%); m.p., decomposition >330 °C; ^{1}H NMR (600 MHz, CDCl$_3$, 25 °C), δ (ppm) 9.03 (s, 2H), 8.41 (d, J = 1.6 Hz, 2H), 7.97 (d, J = 7.6 Hz, 2H), 7.47 (t, J = 7.4 Hz, 2H), 7.35 (t, J = 7.3 Hz, 2H), 7.31 (d, J = 7.5 Hz, 2H), 7.05 (d, J = 2.0 Hz, 2H), 6.67 (s, 2H), 5.81 (s,

2H), 2.74 (s, 6H), 2.32 (s, 6H), 1.22 (br s, 42H), 1.18 (s, 6H); ^{13}C NMR (151 MHz, CDCl$_3$, 25 °C), δ (ppm) 148.39, 146.67, 140.78, 140.03, 137.65, 137.44, 136.17, 134.31, 132.48, 132.16, 130.58, 128.87, 128.61, 127.20, 124.53, 121.42, 121.04, 118.27, 117.04, 104.25, 104.17, 49.28, 21.80, 20.88, 19.34, 18.86, 11.55; HRMS (ES+) (*m/z*), calculated for C$_{68}$H$_{79}$Si$_2$ (M+H)$^+$ 951.5720, found 951.5726; EA calculated for C$_{68}$H$_{78}$Si$_2$ C 85.83%, H 8.26%, found C 85.69%, H 8.18%.

1.4 Synthesis of DIAn

3

DIAn
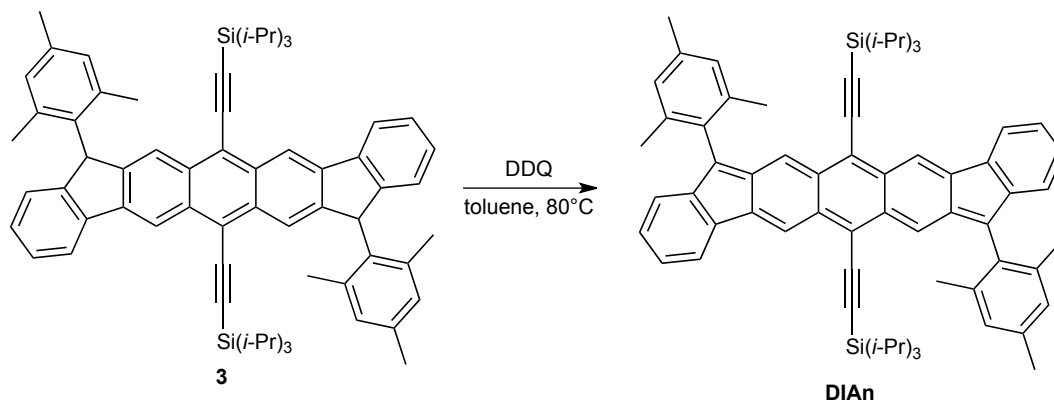
To a 250 ml flask with a stir bar was added **3** (310 mg, 0.26 mmol) and dry toluene (75 ml). The mixture was sparged with N$_2$ for ten minutes then brought to 80 °C. Upon dissolution of **3**, DDQ (89 mg, 0.39 mmol, 1.50 equiv.) in toluene (5 ml) was added dropwise via syringe. After stirring for three hours the deep blue solution was cooled then passed through a plug of basic alumina (4 x 8 cm), eluting with a 1:1 mixture of dichloromethane and hexanes. Volatiles were removed under reduced pressure. The crude material was dissolved in chloroform and an equal volume of acetonitrile was carefully layered above. Dark violet blades of **DIAn** were collected by filtration (192 mg, 62%); m.p., decomposition >260 °C; ^{1}H NMR (600 MHz, CD$_2$Cl$_2$, –25 °C), δ (ppm) 8.41 (s, 2H), 7.72 (d, *J* = 6.3 Hz, 2H), 7.65 (s, 2H), 7.25 – 7.19 (m, 4H), 7.02 (s, 4H), 6.97 (d, *J* = 6.3 Hz, 2H), 2.39 (s, 6H), 2.09 (s, 12H), 1.11 (br s, 42H); ^{13}C NMR (151 MHz, CD$_2$Cl$_2$, –25 °C), δ (ppm) 143.87, 141.89, 138.94, 137.54, 136.85, 136.46, 135.37, 132.54, 130.31, 129.78, 128.73, 128.38, 126.77, 123.54, 123.06, 122.06, 121.58, 121.18, 105.80, 102.34, 21.08, 20.20, 18.53, 11.28; HRMS (ES+) (*m/z*), calculated for C$_{68}$H$_{77}$Si$_2$ (M+H)$^+$ 949.5564, found 949.5536; EA calculated for C$_{68}$H$_{76}$Si$_2$ C 86.02%, H 8.07%, found C 86.06%, H 8.03%.

1.5 NMR spectra

Compound 2 ^{1}H NMR (500 MHz, CDCl$_3$, 25 °C)
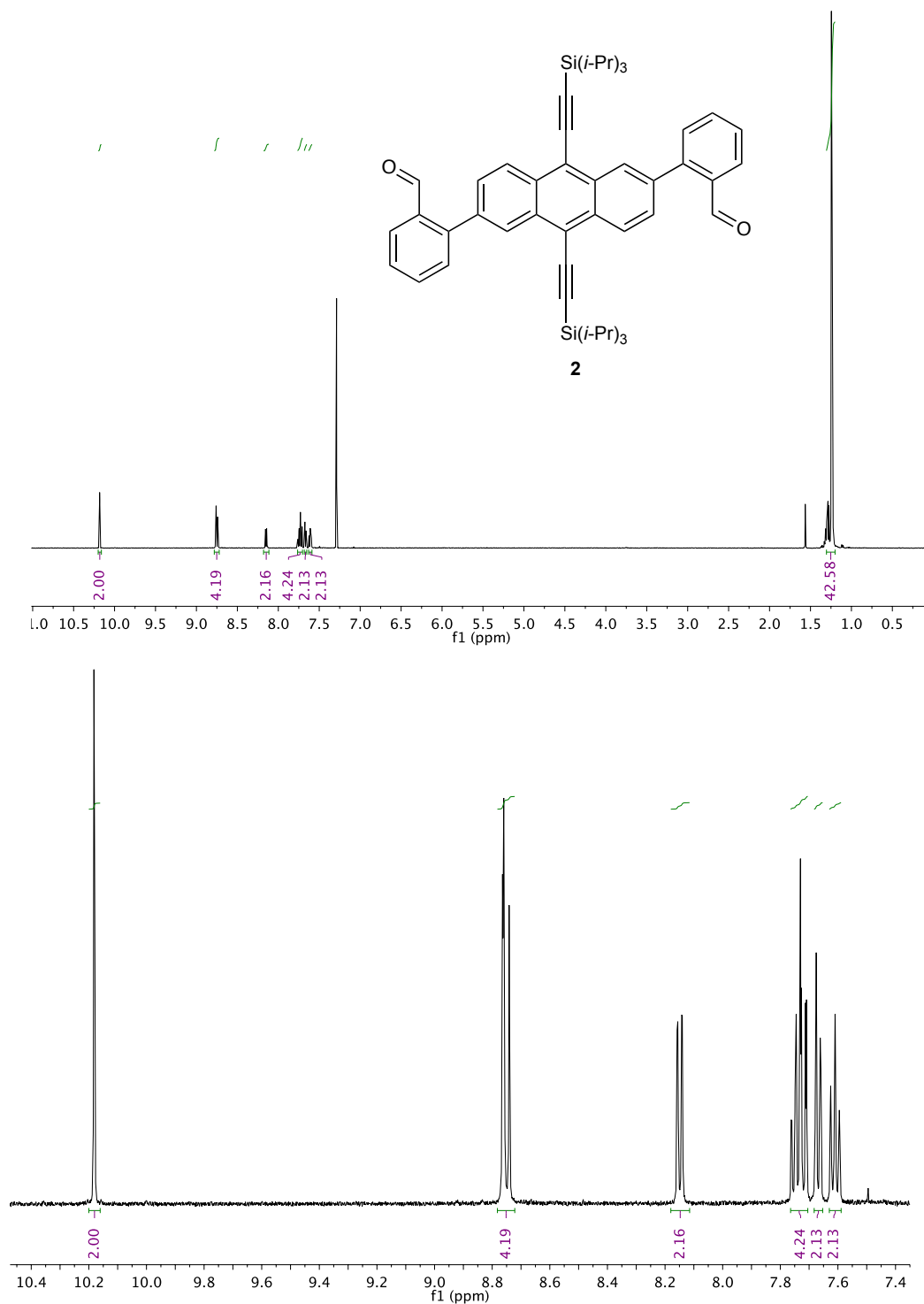
Compound 2 ^{13}C NMR (126 MHz, CDCl$_3$, 25 °C)
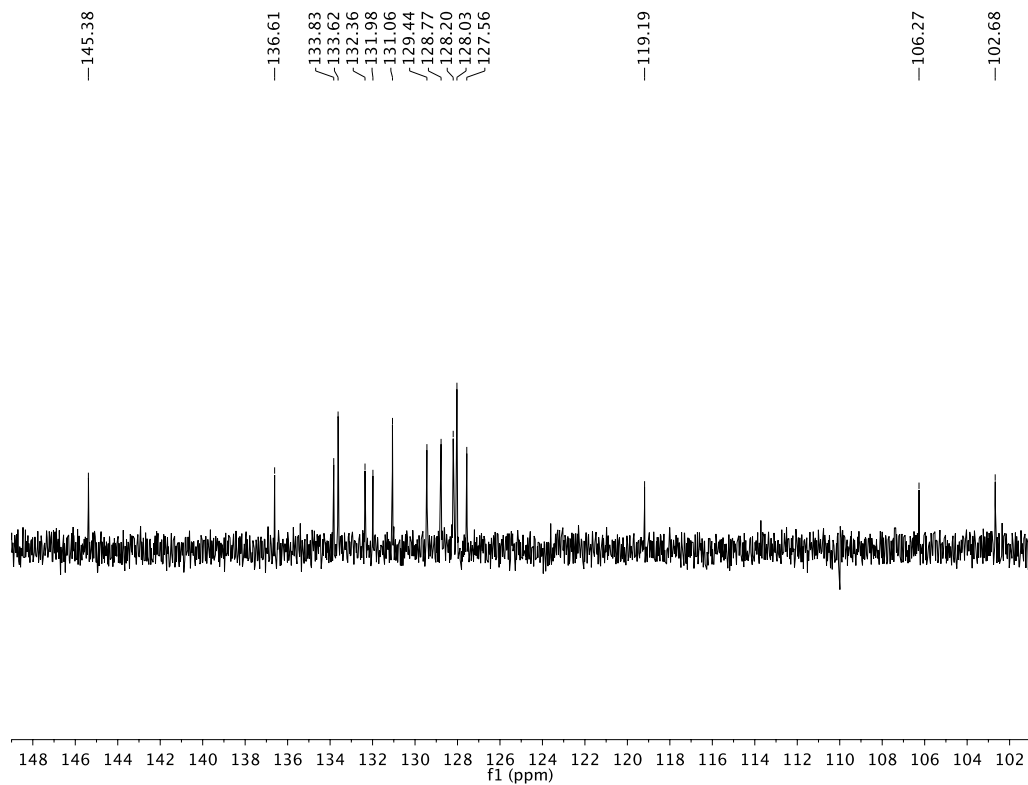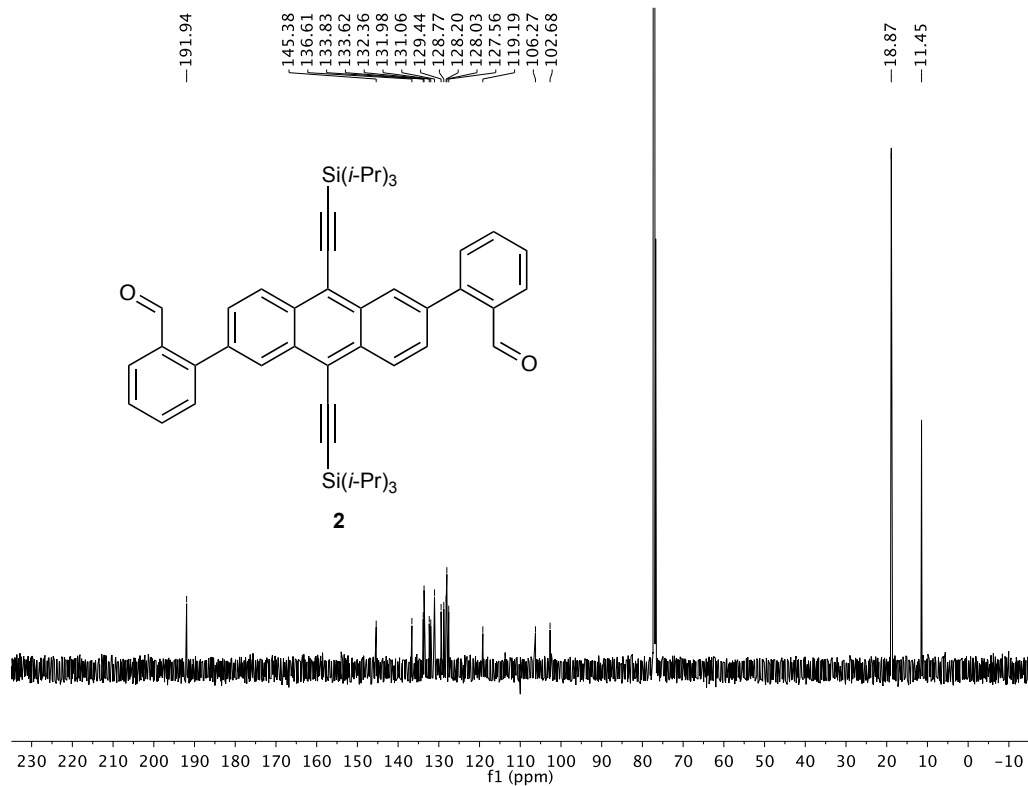
Compound 3 ^{1}H NMR (600 MHz, CDCl$_3$, 25 °C)
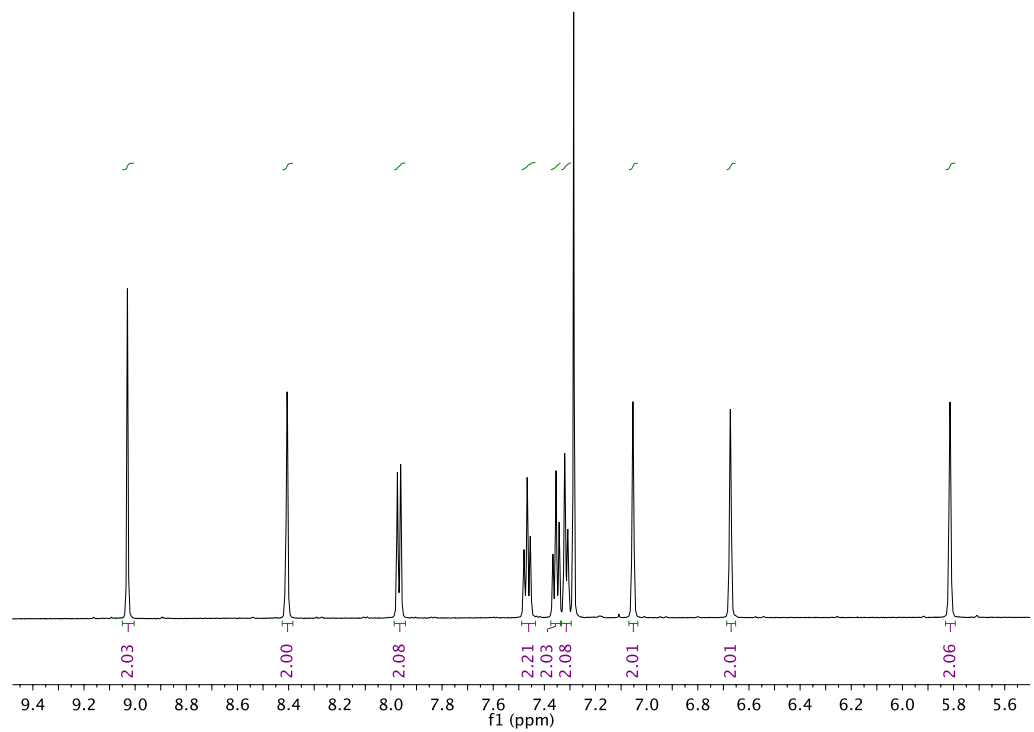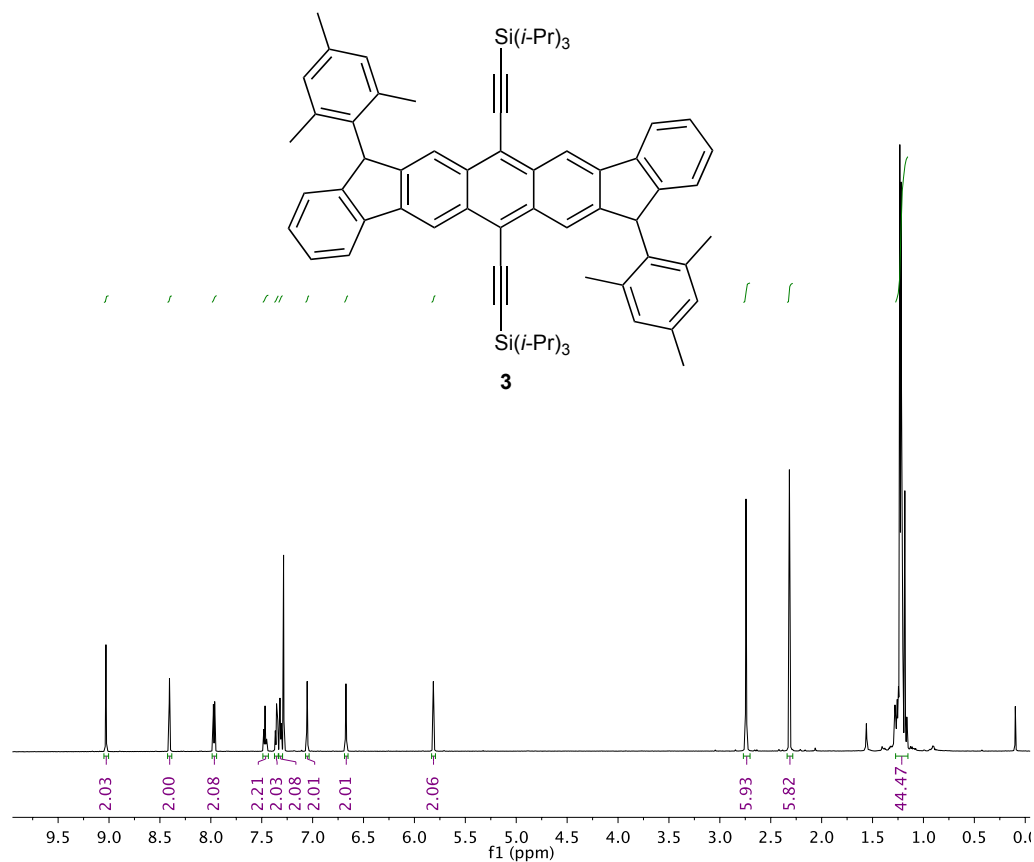
Compound 3 ^{13}C NMR (151 MHz, CDCl$_3$, 25 °C)
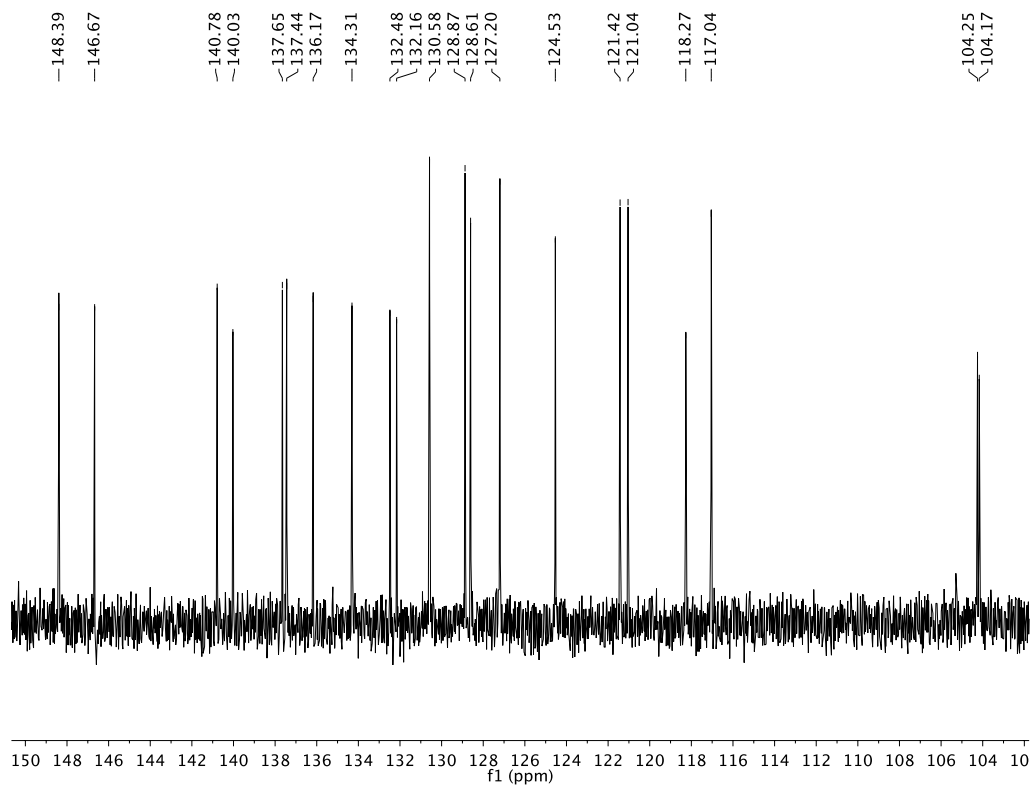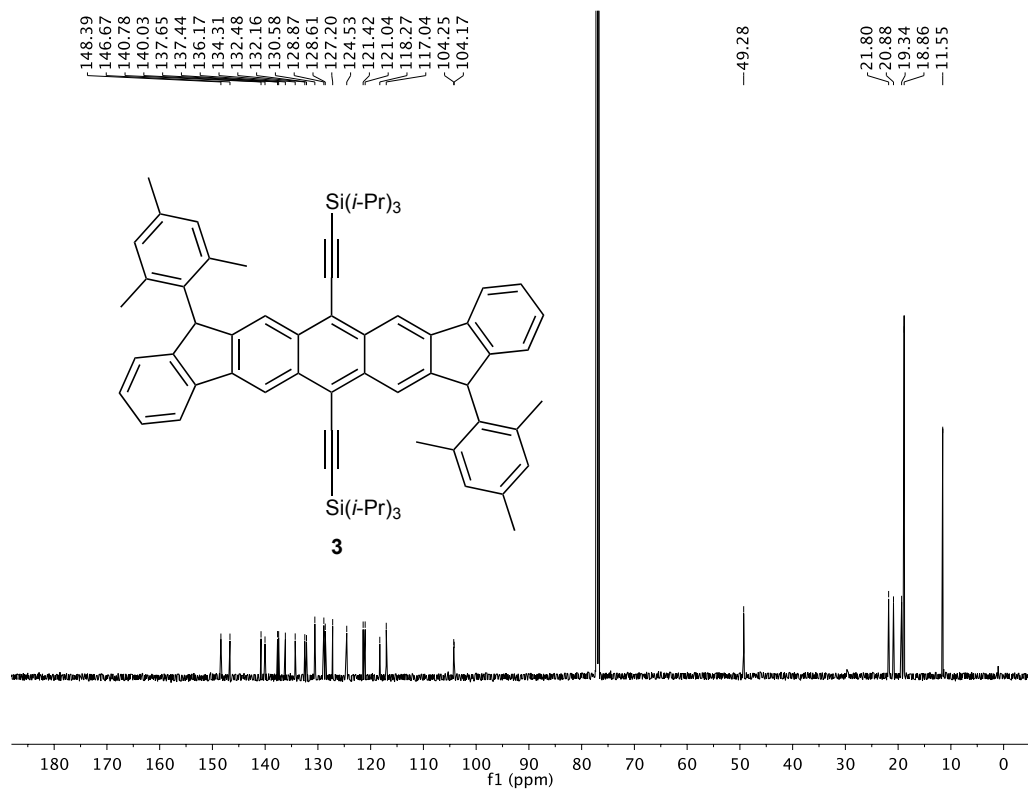
DIAn ^{1}H NMR (600 MHz, CD$_2$Cl$_2$, –25 °C)
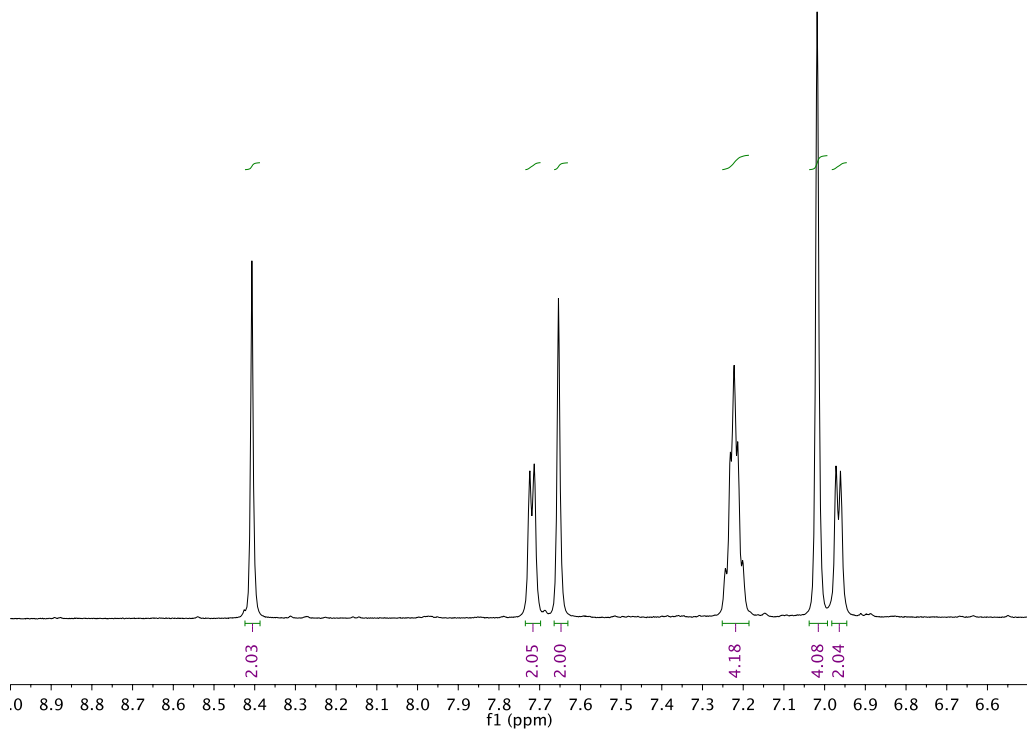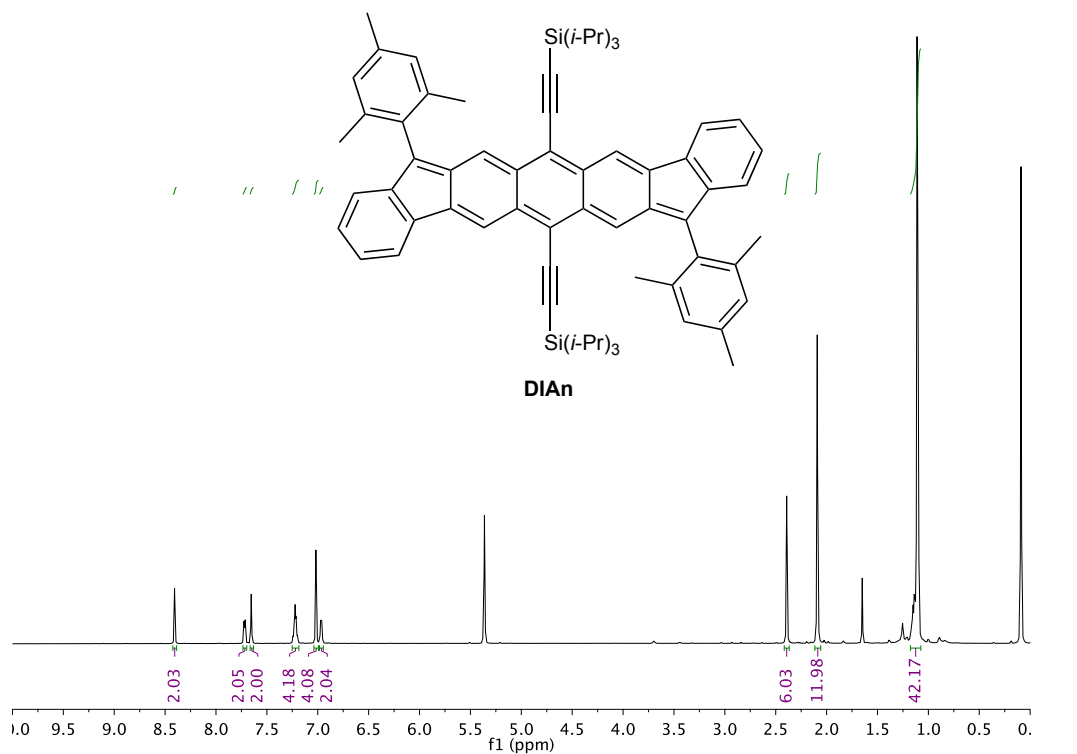
DIAn ^{13}C NMR (151 MHz, CD$_2$Cl$_2$, –25 °C)
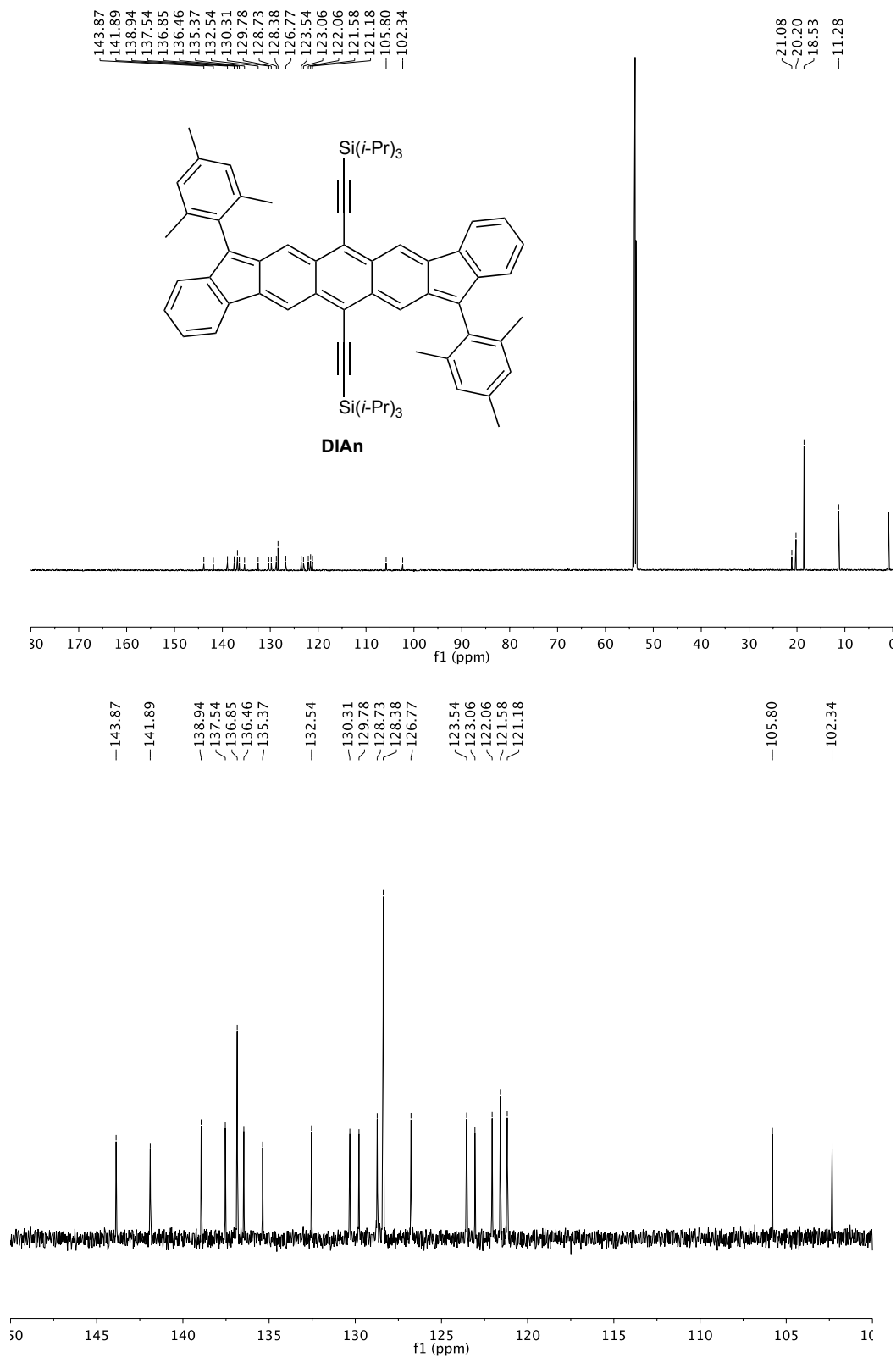
2. Stability experiments

2.1 Quartz cuvette exposed to ambient light

A single crystal of **DIAn** was dissolved in HPLC grade CH_2Cl_2 open to atmosphere. The cuvette was sealed with a Teflon cap and kept on the bench top.
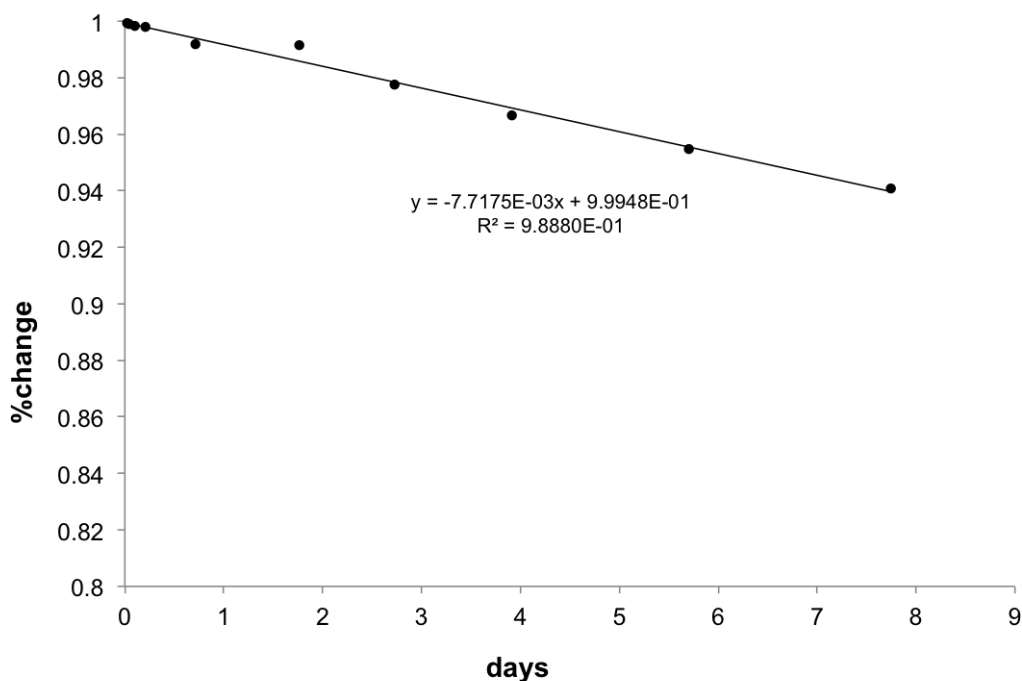
Supplementary Figure 1. Linear regression and extrapolation to % change = 0.50 gives a half-life of 64 days.

2.2 NMR experiment under oxygen

To a J-young tube was added approx. 10 mg **DIAn**, approx. 5 mg 1,3,5-trimethoxybenzene as an internal standard and 0.6 ml $CDCl_3$. The solution was degassed by repeated freeze-pump-thaw cycles. The cap was removed and two balloons of oxygen were sparged through the solution. The tube was resealed and shaken vigorously.
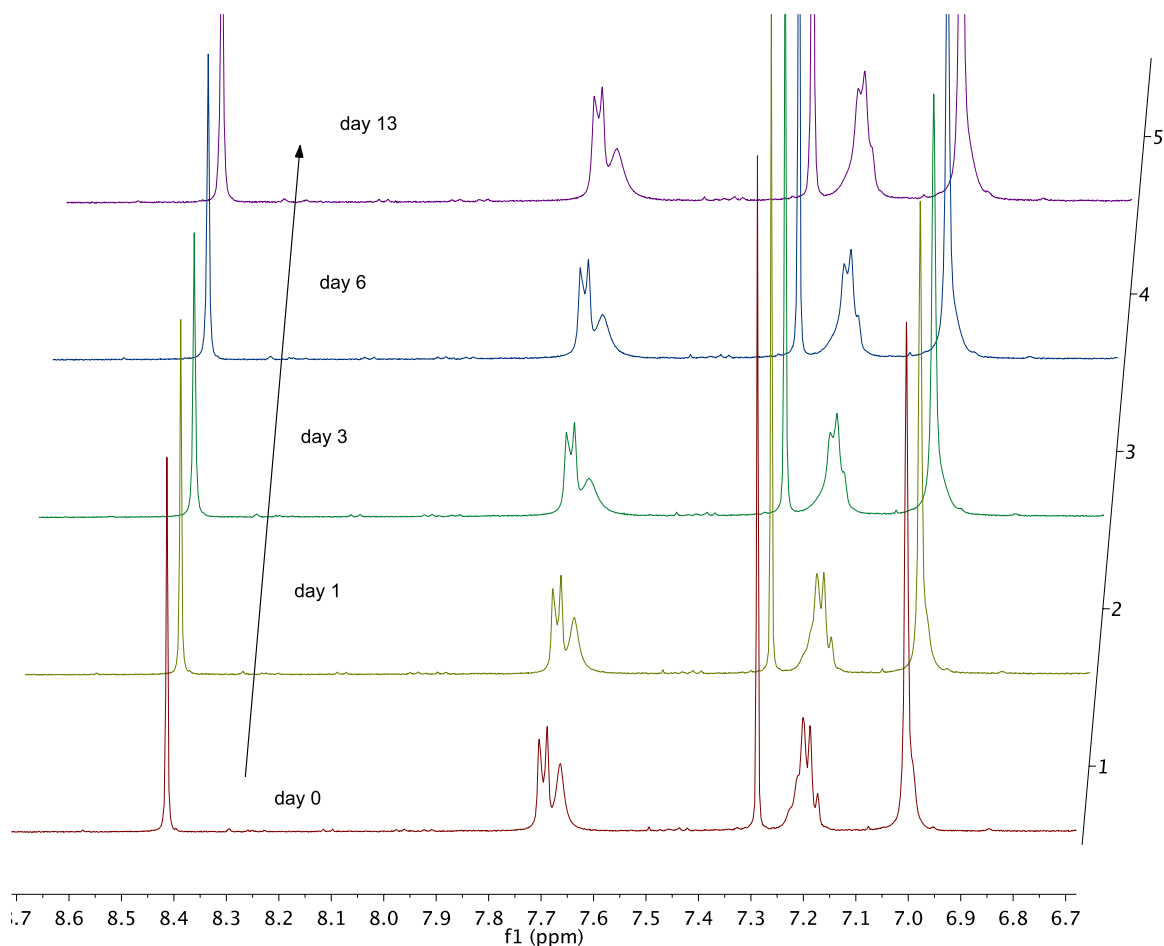
Supplementary Figure 2. NMR spectra show broadening of the **DIAn** aromatic resonances after 13 days. Integration to the internal standard shows no decomposition.

2.3 Thermogravimetric analysis
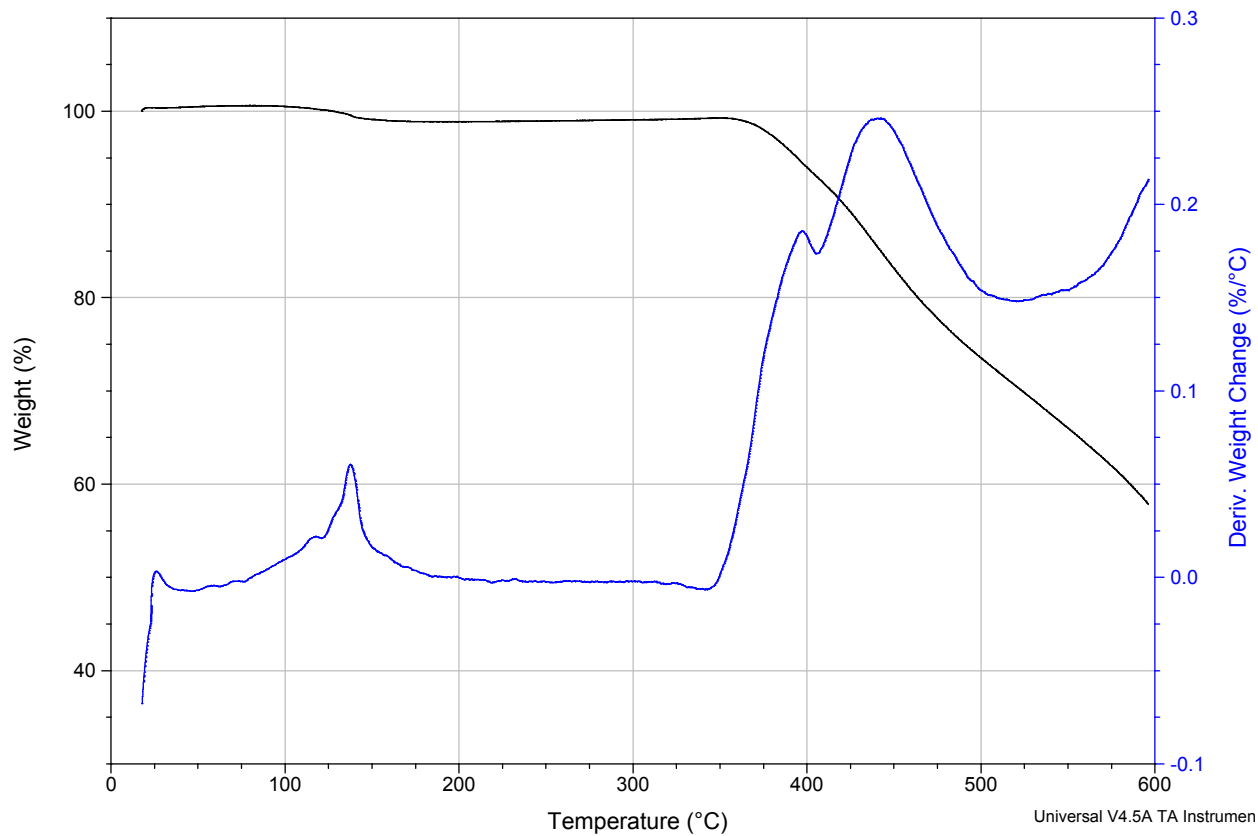
Supplementary Figure 3. TGA of **DIAn** under nitrogen shows negligible decomposition before 350 °C.

3. Cyclic voltammetry

All electrochemical experiments were conducted in a traditional 3-electrode geometry using a Biologic SP-50 potentiostat. Electrolyte solutions (0.1 M) were prepared from HPLC grade DCM and anhydrous Bu_4NBF_4, and the solutions were degassed via freeze-pump-thaw (3×) prior to analysis. The working electrode was a glassy carbon electrode (3 mm diameter) with a Pt-coil counter electrode and Ag wire pseudo reference. The ferrocene/ferrocenium (Fc/Fc^+) couple was used as an internal standard following each experiment. Potential values were re-referenced to SCE using a value of 0.46 (V vs. SCE) for the Fc/Fc^+ couple in CH_2Cl_2. When necessary, potentials were re-referenced to NHE using SCE = –0.24 (V vs. NHE). LUMO and HOMO levels were approximated using SCE = –4.68 eV vs. vacuum.[2] Cyclic voltammetry experiments were conducted in a nitrogen-filled drybox at sweep rates of 50 (reported), 75, 100, 125 and 150 mV s^{-1}. All scan rates show quasi-reversible kinetics with no alteration of peak splitting with scan rate. $E_{1/2}$ values were calculated assuming $E^{o'} \approx E_{1/2} = (E_{anodic} + E_{cathodic})/2$ based on these observations for reversible couples. The $E_{a,c}$ peak splitting of the Fc/Fc^+ couple was similar to that of the analyte (~100 mV). The anodic peak current increases linearly with the square root of the scan rate in the range 50 to 150 mV s^{-1}, indicating a diffusion-controlled process. Analyte concentrations were ca. 1–5 mM.

4. X-Ray crystallography

4.1 General X-Ray data collection

Diffraction intensities were collected at 173 K on a Bruker Apex2 CCD diffractometer using MoKα radiation, λ= 0.71073 Å. Space group was determined based on systematic absences. Absorption correction was applied by SADABS.[3] Structure was solved by direct methods and Fourier techniques and refined on F^2 using full matrix least-squares procedures. All non-H atoms were refined with anisotropic thermal parameters. H atoms were treated in calculated positions. Diffraction data were collected up to $2\theta_{max}$ = 56.0° and have been used in the final refinement. All calculations were performed by the SHELXL-2013 package.[4] *Crystallographic Data for* **DIAn**: $C_{68}H_{76}Si_2$, M = 949.46, 0.19 × 0.19 × 0.13 mm, T = 173 K, Monoclinic, space group $P2_1/c$, a = 12.3601(12) Å, b = 14.0292(13) Å, c = 16.6209(16) Å, β = 97.754(3)°, V = 2855.8(5) Å^3, Z = 2, Z' = 0.5, D_c = 1.104 Mg/m^3, μ(Mo) = 0.102 mm^{-1}, F(000) = 1024, $2\theta_{max}$ = 56.0°, 32693 reflections, 6932 independent reflections [R_{int} = 0.0503], R1 = 0.0555, wR2 = 0.1370 and GOF = 1.029 for 6932 reflections (316 parameters) with I>2σ(I), R1 = 0.0957, wR2 = 0.1645 and GOF = 1.029 for all reflections, max/min residual electron density +0.391/–0.363 eÅ^{-3}. CCDC-1426708 contains the supplementary crystallographic data for this compound. The data can be obtained free of charge from the Cambridge Crystallographic Data Centre via www.ccdc.cam.ac.uk/data_request/cif.

4.2 Solid-state arrangement of DIAn
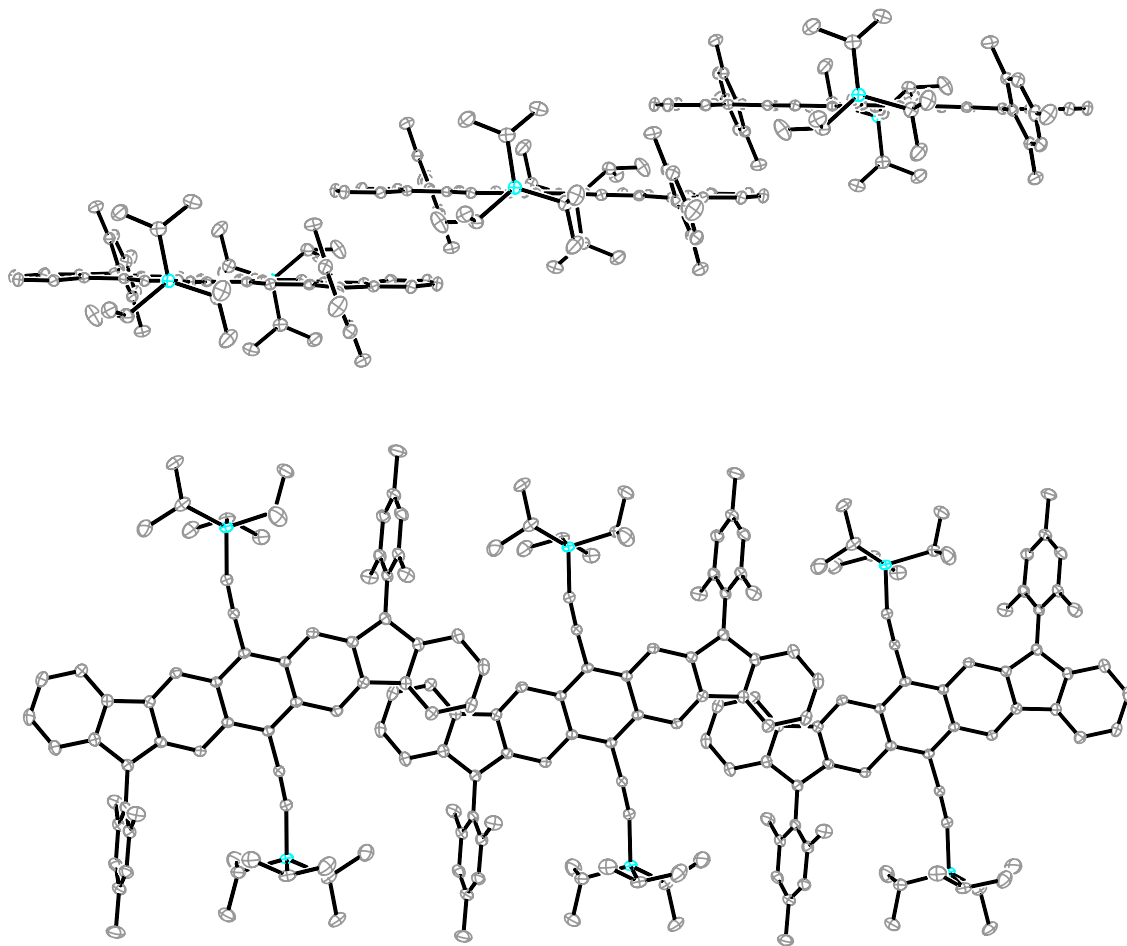
Supplementary Figure 4. ORTEP images showing the solid state packing of **DIAn** drawn with 35% thermal ellipsoids, hydrogens are omitted for clarity.

5. Variable-temperature NMR experiment

Approximately 10 mg of **DIAn** was dissolved in 1,2-dichlorobenzene-d_4 and transferred to a J-Young tube. The solution was degassed by 4 freeze-pump-thaw cycles. Spectra were acquired in a Varian Inova 500MHz spectrometer that was heated to 50, 75, 100, 125, 150, then 25 °C.
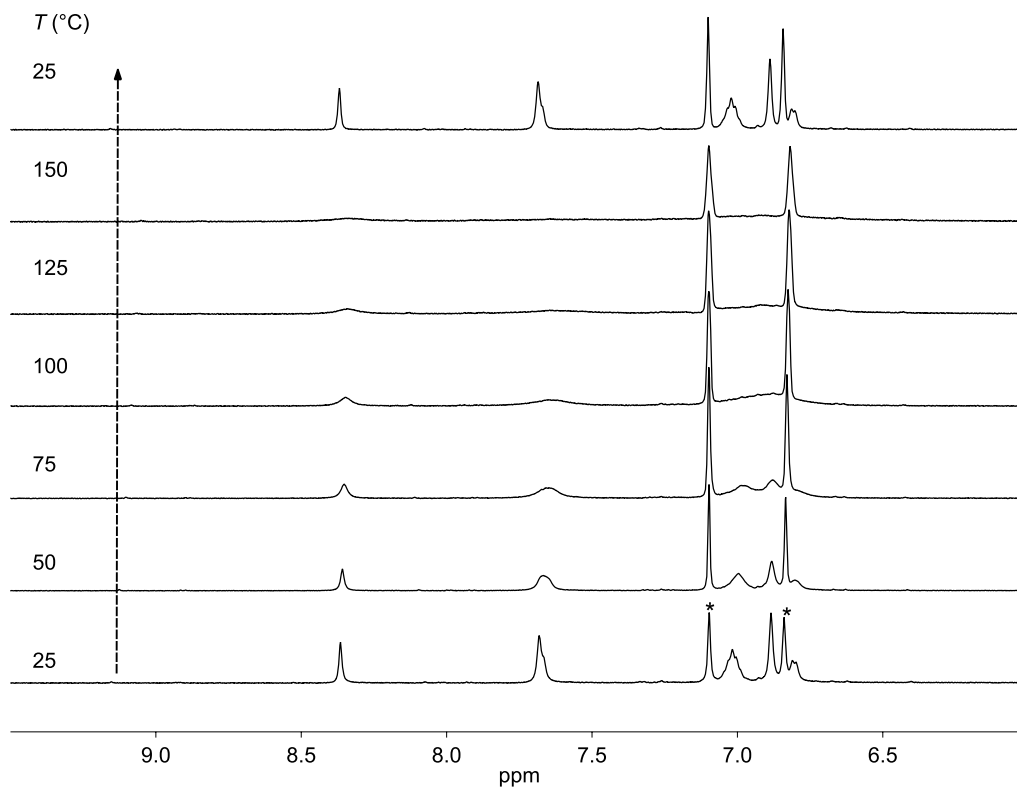
Supplementary Figure 5. VT ^{1}H NMR spectra of the aromatic region of **DIAn** in 1,2-dichlorobezene-d_4, residual non-deuterated ODCB solvent (*).

Supplementary Figure 6. VT ^{1}H NMR spectra of the aliphatic region of **DIAn** in 1,2-dichlorobezene-d_4.

Supplementary Figure 7. Proton NMR spectrum of the high-temperature experiment 28 days later showing negligible decomposition.

6. Raman spectroscopy

6.1 General details

Raman spectra were recorded in the solid state in off- or on-resonance conditions depending on the excitation wavelength used, either 785 or 633 nm. The measurements were carried out in the 1×1 camera of a Bruker Senterra Raman microscope by averaging spectra during 50 min with a resolution of 3–5 cm^{-1}. A CCD camera operating at -50 °C was used for detection. Variable temperature Raman measurements were performed in KBr pellets (to assure faster thermal equilibration) in the range between 25 and 150 ºC, by using a Linkam FTIR600 stage cooled by liquid nitrogen and with a temperature stability of <0.1 °C.
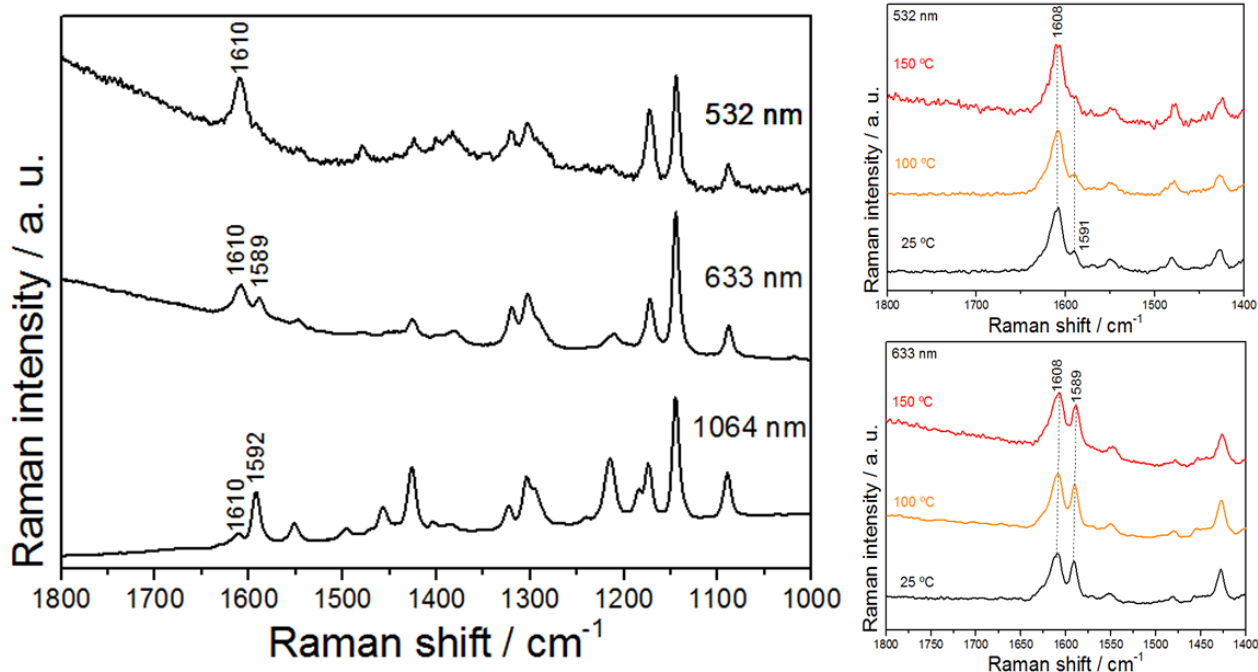
Supplementary Figure 8. Raman spectra of solid DIAn taken with several Raman excitation wavelengths (left) and variable temperature Raman spectra of DIAn with several Raman excitation wavelengths (right).
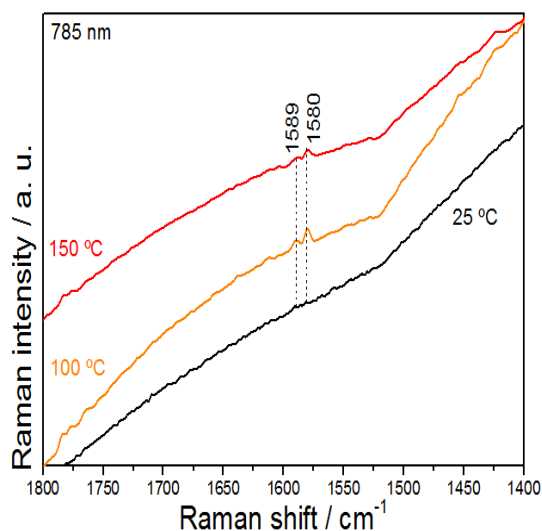
Supplementary Figure 9. The full region where the aromatic/quinoidal C=C stretching frequencies in the 1800-1400 cm^{-1} range is shown; spectra taken with the 785 nm Raman excitation wavelength at different temperatures.

6.2 Comparison between Raman spectra of DIAn and its corresponding dihydrogenated presursor

Supplementary Figure 10 displays the Raman spectra of **DIAn** in its singlet open-shell pseudo-aromatic state and in its low energy lying aromatized triplet excited state (recorded at 150 ºC) together with the Raman spectrum of the dihydrogenated precursor, **DIAn-H$_2$** (compound **3**), also in the solid state. This precursor (see chemical structure in Supplementary Figure 11 below) contains a fully aromatized anthracene moiety with the external benzenes partially decoupled from the anthracene core. Hence, **DIAn-H$_2$** can be used as a reference compound to address the effect or degree of aromatization in the central core of **DIAn**. In **DIAn-H$_2$**, there are two neat bands at 1580 cm^{-1} which is due to the CC stretching vibration of the central anthracene core; thus, it can be considered as typical of an aromatized structure. At higher frequencies, 1606 cm^{-1}, the second band appears which is due to the CC stretching of the external benzene rings. Therefore, the band at 1580 cm^{-1} in the spectrum of the triplet excited state corroborates its aromatic character in the central anthracene. On the other hand, the 1589 cm^{-1} band in the singlet ground electronic state of **DIAn** due to the CC stretching of the central core corroborates its partial aromatized character in contrast with the more accentauted character of the aromatic shape in the triplet.
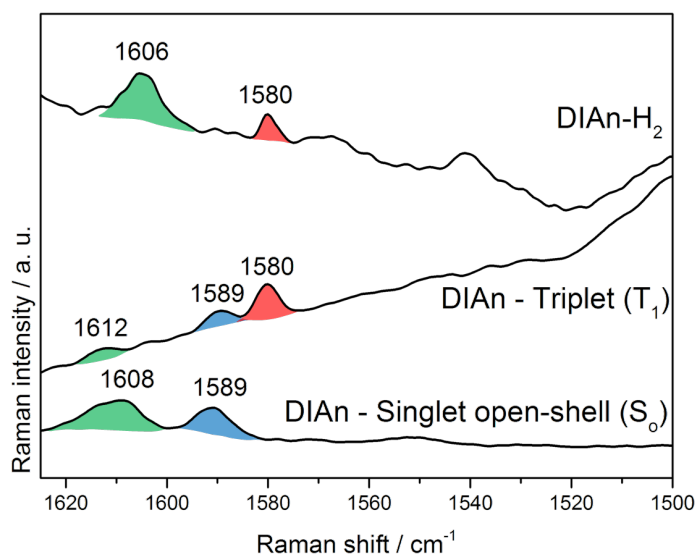
Supplementary Figure 10. Bottom: solid-state Raman spectrum of **DIAn** (633 nm, 25 °C). Middle: solid-state Raman spectrum of **DIAn** (785 nm, 150 °C). Top: solid-state Raman spectrum of **DIAn-H$_2$** (785 nm, 25 °C).
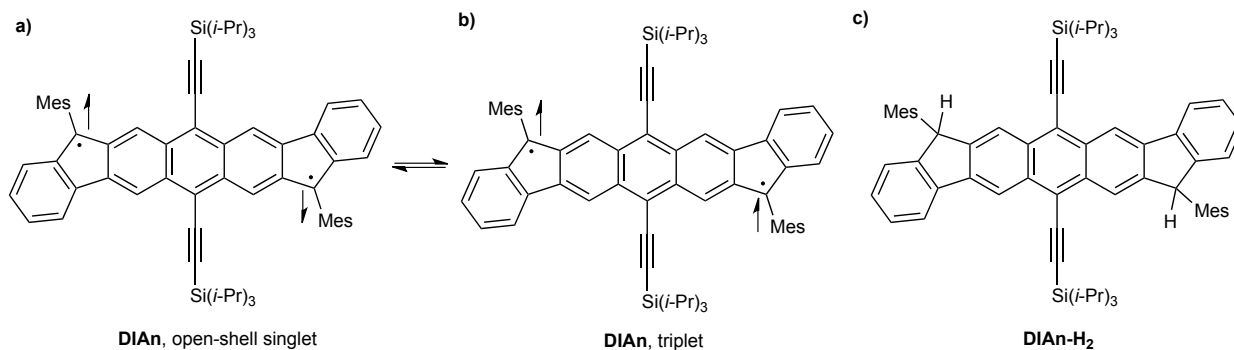
Supplementary Figure 11. Resonance structures of **DIAn**: a) open-shell singlet and b) triplet. c) Chemical structure of **DIAn-H$_2$** (compound **3**).

7. ESR measurements

The X-band ESR measurements were performed on a polycrystalline powder sample in the 4.2-300 K temperature range with a Q-band (34.0 GHz) Bruker ELEXSYS E580 Spectrometer equipped with a helium cryostat (Supplementary Fig. 12a). The spin susceptibility (proportional to the area of the signal) was obtained by integrating the area of the signal at each temperature. In this way it was possible to obtain a qualitative variation of the spin susceptibility with temperature (Supplementary Fig. 12b). As expected, this thermal variation can also be reproduced with the classical Bleaney-Bowers model although, given the qualitative character of these measurements, the obtained J value is lower than the one obtained from the SQUID measurements.

a

b
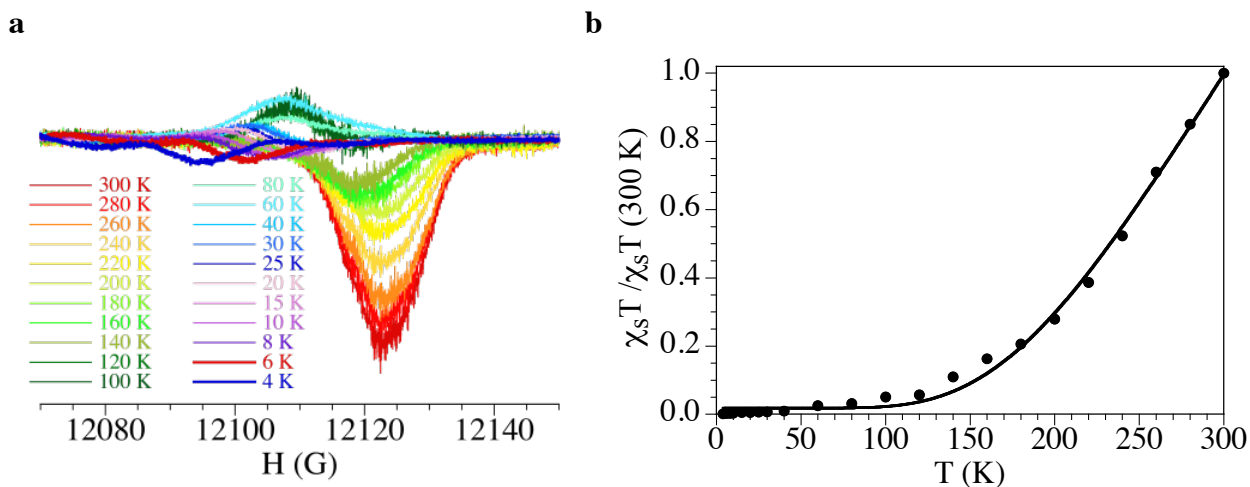
Supplementary Figure 12. **a**, Solid-state ESR spectra taken from 300K to 4K. **b**, Thermal variation of the normalized product of the EPR spin susceptibility times the temperature for the title compound. Solid line is the best fit to the Bleaney-Bowers model.

8. SQUID measurements

The magnetic susceptibility measurements were carried out in the temperature range 2–400 K with an applied magnetic field of 0.1 T on a polycrystalline sample of the title compound (with a mass of 9.88 mg) with a Quantum Design MPMS-XL-5 SQUID susceptometer. The susceptibility data were corrected for the sample holder previously measured using the same conditions and for the diamagnetic contribution of the compound as deduced by using Pascal´s constant tables. The experiental data (χ_mT vs. T) were fit using the classical Bleaney-Bowers model for an antiferromagentic S = ½ dimer:[5]

$$\chi_m = \frac{2Ng^2\beta^2}{k_BT} \frac{1}{3 + exp\left(-J/k_BT\right)}$$

9. Computational details

9.1 Geometry optimization

To perfom the computational investigation of the synthesized **DIAn** derivative, we adopted two model systems, **DIAn-a** and **DIAn-b** (Supplementary Fig. 13). For all the calculations, the 6-311G(d) basis set is applied. Gaussian 09 program package is applied for all the calculations except for the spin-flip TD-DFT calculations.[6] GAMESS and Q-CHEM program packages are applied for the calculation of spin-flip calculation with the collinear and the non-collinear kernels, respectively.[7,8]

DIAn-a, R^1 =   R^2 = ―――――SiMe$_3$

DIAn-b, R^1 = R^2 = H
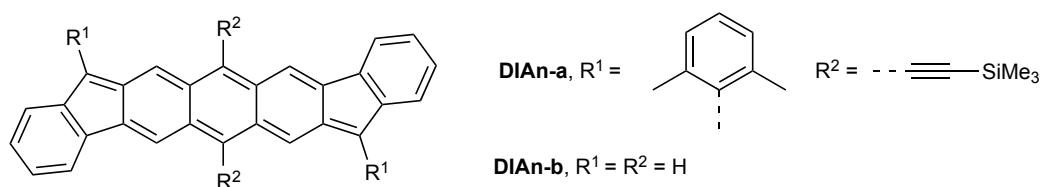
Supplementary Figure 13. Model structures used in computations.

For the geometry optimization of the model systems, restricted and unrestricted B3LYP method for both the model systems and spin-flip TD-BHHLYP for only **DIAn-b** have been adopted and the obtained geometries were compared to the experimentally obtained X-ray crystallographic data. All the optimized geometries were confirmed to be at the potential energy local minima by the hessian calculation. Supplementary Figure 14 shows the numbering scheme of the bonds in π-conjugated framework and the bond length alternation is shown in Supplementary Figure 15 for the singlet states and in Supplementary Figure 16 for the triplet states.
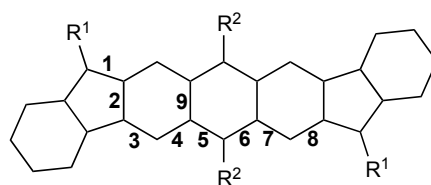
Supplementary Figure 14. **DIAn** model system numbering scheme.
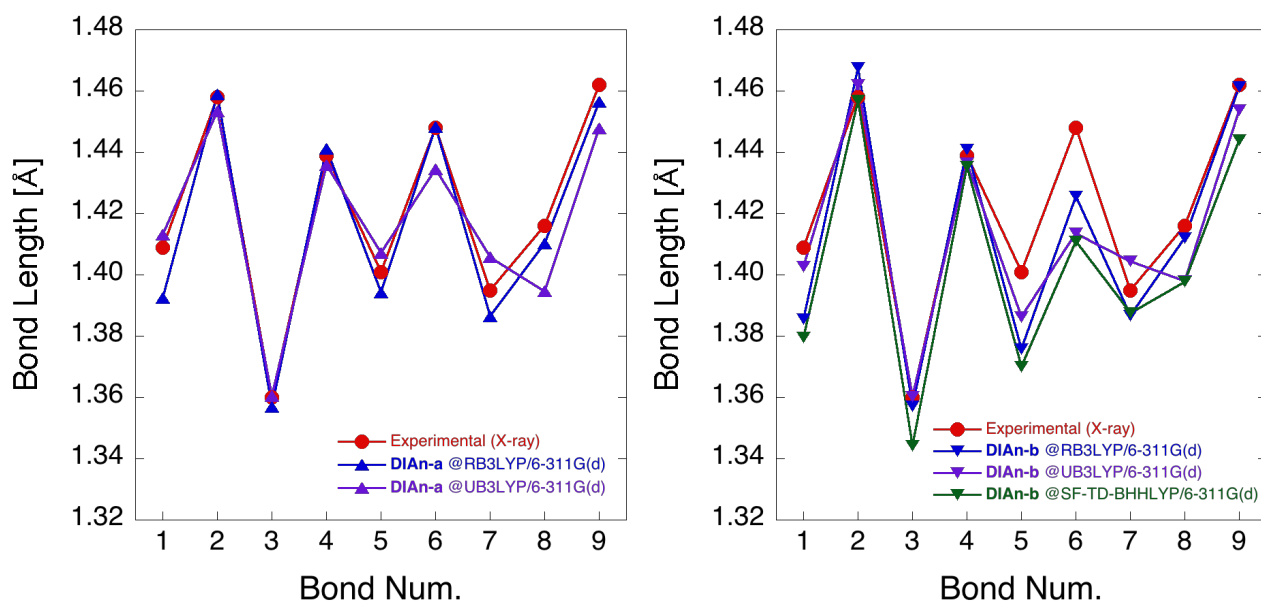
Supplementary Figure 15. Bond length alternation of the π-conjugated framework in the singlet states.

The **DIAn-a** geometry optimized at RB3LYP/6-311G(d) level of theory reproduces the bond length and also the alternation of the experimental data quite well. Also, the smaller **DIAn-b** optimized at RB3LYP semi-qualitatively agrees well though the bonds 5 and 6 are shorter than those of **DIAn-a**, the differences of which originate from the existence/absence of the bulky substituents. The validity of the optimization at RB3LYP method is also confirmed with the fact the bond length alternation is in semi-quantitatively well agreement with the optimized geometry of **DIAn-b** at the spin-flip TD-BHHLYP method, which is known to well reproduce the geometries of diradical species.[9] On the other hand, the UB3LYP method fails to reproduce the bond length alternation of the singlet species even in qualitative manner for both the model systems though the method is often adopted for the calculations of open-shell species (see bond 7 to 8). This is probably because of the spin contamination error of the unrestricted wavefunctions. In fact, this tendency of the optimized geometry that the bond 7 is shorter than that of the bond 8 is the tendency observed in the triplet states even at the spin-flip TD-BHHLYP method (Supplementary Fig. 16). For the triplet geometry, the UB3LYP method well reproduces that of the spin-flip TD-BHHLYP method for the **DIAn-b**. **DIAn-a** in the triplet state optimized at UB3LYP method agrees well with that of the **DIAn-b** except for the bonds 5 and 6, which is lengthened by the substitution groups. The reason why the triplet geometry of the spin-flip TD-BHHLYP method is well reproduced by the UB3LYP method would be the negligible spin

contamination of the unrestricted wavefunction in the triplet state. From these observations, we adopt the **DIAn-a** structure optimized at RB3LYP method for the singlet state and UB3LYP method for the triplet state for the further investigations.
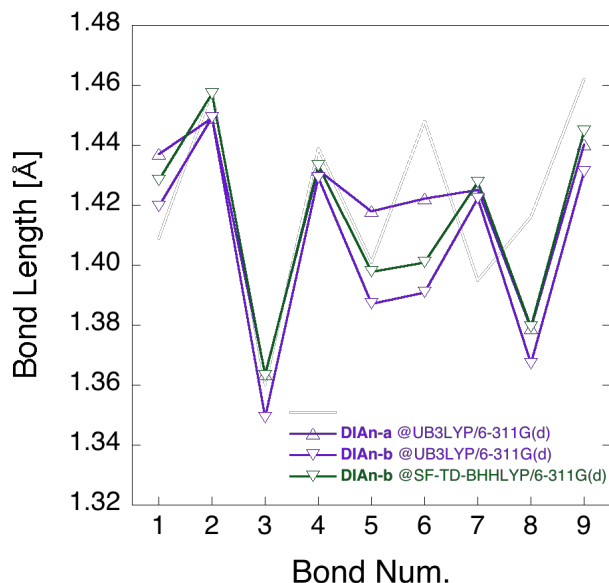
Supplementary Figure 16. Bond length alternation of the π-conjugated framework in the triplet states.

The open-shell singlet solution is the lowest energy state of **DIAn**; however, unrestricted DFT calculations sometimes cause severe problem on the geometry optimization because of the spin contamination error. The validity of the optimized geometry is confirmed above by the comparison with the X-ray data but also with the higher level of theory with negligible spin contamination error, spin-flip TD-DFT method. The energies of open-shell (singlet in unrestricted), closed-shell (singlet in restricted) and triplet (triplet in unrestricted) at B3LYP/6-311G(d) level of theory using the RB3LYP/6-311(d)-optimized geometry are given in Supplementary Table 1.

Supplementary Table 1. Relative energy (kcal mol^{-1}) of **DIAn-a** and **DIAn-b** at B3LYP/6-311G(d) level of theory using the singlet optimized geometry by the RB3LYP/6-311G(d) method.

	DIAn-a	DIAn-b
open-shell singlet, unrestricted	(set as 0)	(set as 0)
open-shell triplet, unrestricted	8.30	9.50
closed-shell singlet, restricted	1.44	1.07

9.2 Singlet-Triplet energy gap and biradical character index, y, calculation

The singlet–triplet energy gap (ST gap) accompanied with the geometry relaxation is calculated using the zero point vibration energy at the same level of theory as the optimization and the electronic energy of each optimized geometry calculated at the spin-flip TD-PBE50 method with the non-collinear kernel.[10] The calculated ST gap is 4.9 kcal mol^{-1} including the difference of the zero-point vibration energies of 0.9 kcal mol^{-1}. The result quite well agrees with the experimentally determined ST gap, 4.18 kcal mol^{-1}.

The open-shell character of the present system is characterized with the spin-projected unrestricted hartree-fock (PUHF) method, which well reproduces the variation in the diradical character of H_2 dissociation calculated at the full configuration interaction method.[11] Within the PUHF method, the diradical character is expressed as the following equation:

$$y = 1 - \frac{2T}{1+T^2} ,$$

where T indicates the orbital overlap between the highest occupied natural orbital (HONO) and the lowest unoccupied natural orbital (LUNO). Using the occupation numbers of UHF natural orbitals (UNO), the overlap T is calculated as follows:

$$T = \frac{n_{HONO} - n_{LUNO}}{2} ,$$

Since the diradical character is not an observable and is an index of "the degree" of the open-shell singlet character, the absolute value varies with the calculation method, but once the

calculation method is determined, the y value can be compared each other. In this regard, one should be careful on which calculation method is used for the determination of the diradical character when comparing y with some other one calculated at the other study. Therefore, to compare the diradical character of the present system with the previously synthesized open-shell systems, we have recalculated the four simplified model systems of the reported open-shell singlet systems, indeno[2,1-*b*]fluorene, indacenodiphenalene, octazethrene and teranthene, at the method applied in the present study. The result shows that the diradical character of these systems is in the range between 0.504 and 0.737 (Supplementary Fig. 17).
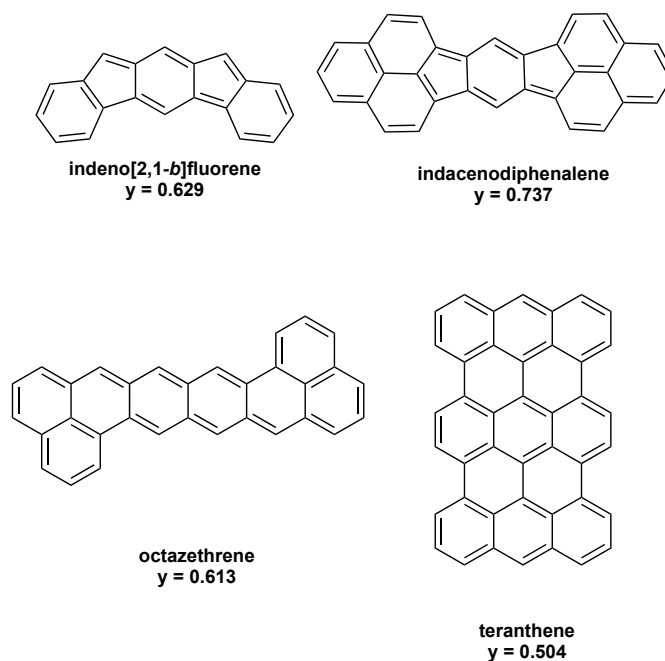
Supplementary Figure 17. Comparison of open-shell PCHs with calculated biradical character index y.

The spatial distribution of the open-shell character is expressed with the odd-electron density distribution;[12]

$$\rho^{\text{odd}} = y \times \left\{ \left| \phi_{\text{HONO}} \right|^2 + \left| \phi_{\text{LUNO}} \right|^2 \right\}.$$

Since in the present case, we apply LC-UBLYP method for the calculation of the odd-electron density, the applied y in the above equation is calculated without spin-projection scheme. Namely, we apply the occupation number of LUNO in the LC-UBLYP method as y for the calculation of the odd-electron density distribution.

9.3 NICS-XY scans and ACID plots calculations

The NICS-XY scans[13] were performed using Gaussian09 Rev. D.01 and Aroma 1.0.[14] We used the B3LYP[15] functional as well as LC-BLYP combining the BLYP functional[16] with the long-range correction of Hirao[17], both together with the 6-311+G(d,p) basis set.[18] For the LC scheme a "ω" value of 0.33 was employed by specifying the following keywords in Gaussian09: "iop(3/107=0330000000,3/108=0330000000)". The GIAO[19] procedure was employed for the calculation of the NICS values at 1.7 Å above the molecular plane and the σ-only model[20] was used to remove the influence of the σ system. Minima with substantially negative NICS values in the NICS-XY scan represent aromatic rings, while maxima with substantially positive values represent antiaromatic rings. NICS values around zero correspond to non-aromatic rings. For benzene, the minimum NICS value at 1.7 Å distance above the ring plane is –16 ppm with the σ-only model, while the maximum value for D_{2h} cyclobutadiene is ca. +20 ppm.[13]

The ACID[21] plots were generated with Gaussian09 using the CSGT method[22] and AICD 2.0.0. ACID is a method to visualize conjugation and ring currents in molecules. Clockwise ring currents correspond to aromatic systems and counter-clockwise ring currents to antiaromatic systems. Systems with no evident ring current are considered non-aromatic. The following keywords were used in Gaussian09 to control the grid size for the GIAO and CSGT calculations: "cphf=grid=fine" and "integral=grid=ultrafine".

The NICS-XY scan for **DIAn-b** with B3LYP is presented in Supplementary Figure 18. The LC-UBLYP ACID plot for the T_1 state of **DIAn-a** is presented in Supplementary Figure 19, while the ACID plots for S_0 and T_1 with B3LYP are found in Supplmentary Figures 20 and 21, respectively. The results with B3LYP and LC-UBLYP are in general agreement, although LC-UBLYP ascribes a larger open-shell character to the singlet state. It has previously been shown that LC-UBLYP better reproduces optical response properties of open-shell species as compared to B3LYP.[23]
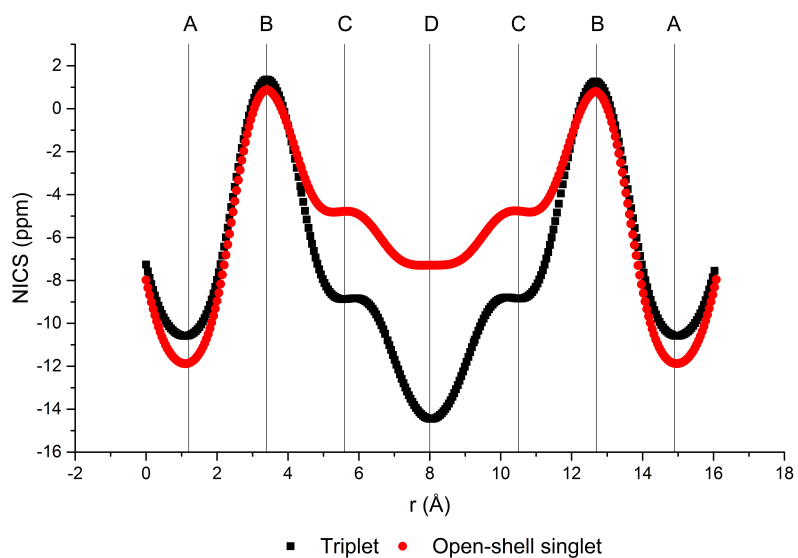
Supplementary Figure 18. GIAO-UB3LYP/6-311+G(d,p) NICS-XY scan comparing open-shell singlet and triplet states of **DIAn-b**.
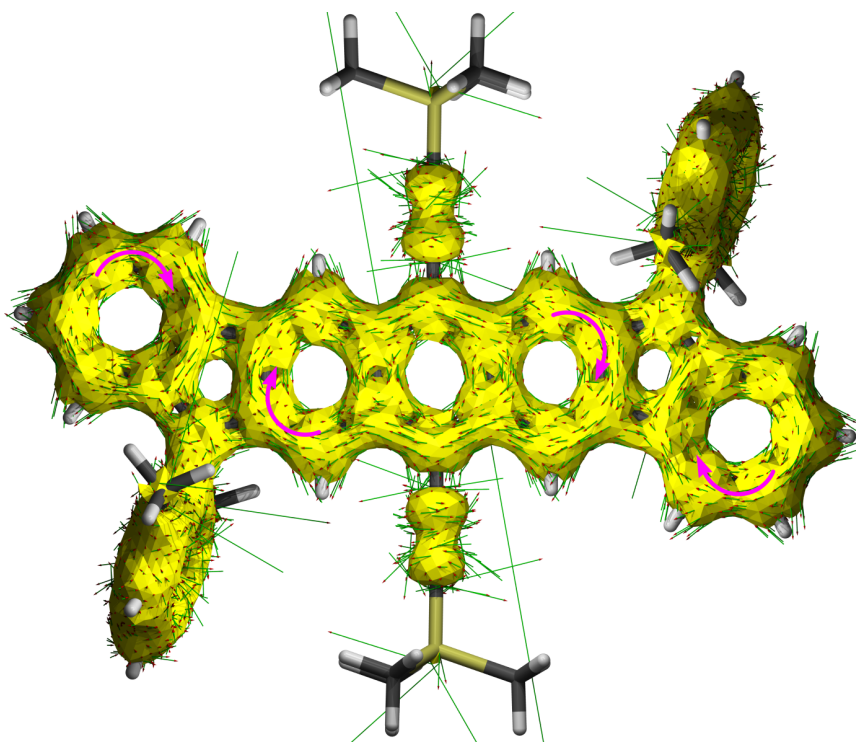
Supplementary Figure 19. ACID plot in T_1 at the LC-UBLYP/6-311+G(d,p) level of **DIAn-a**.
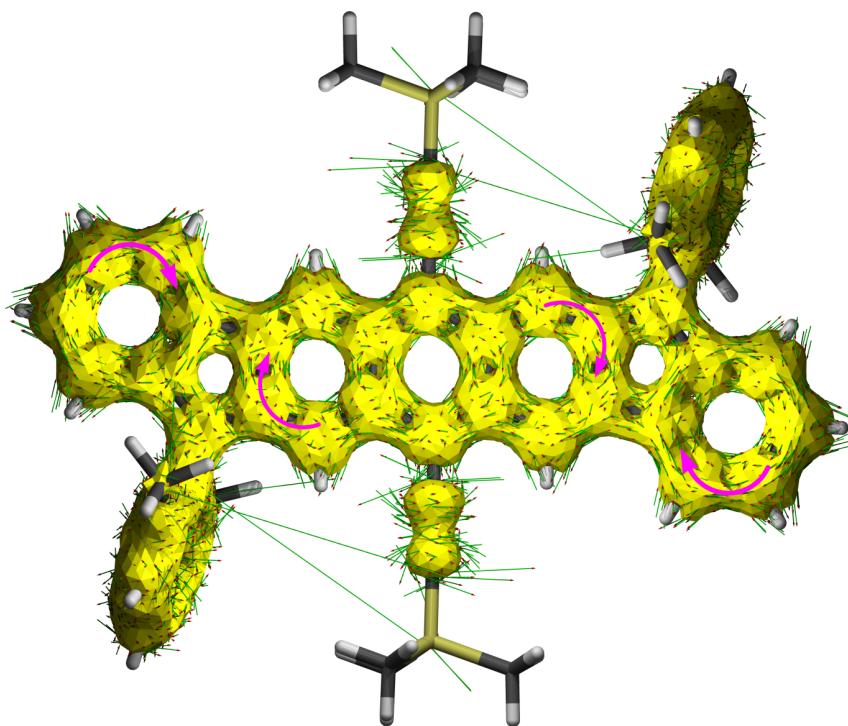
Supplementary Figure 20. ACID plot in S_0 at the UB3LYP/6-311+G(d,p) level of **DIAn-a**.
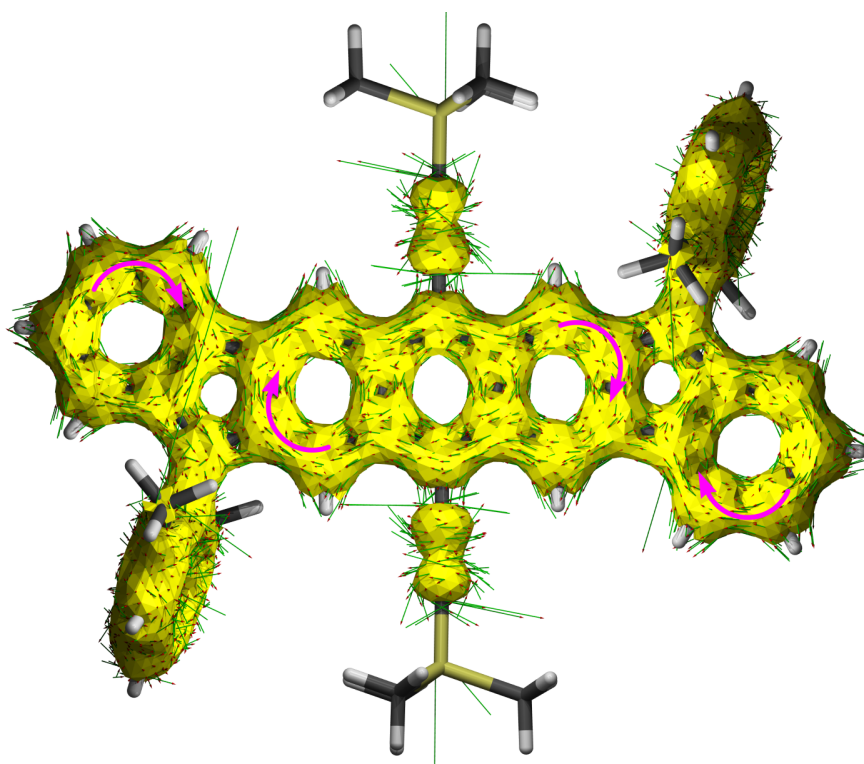
Supplementary Figure 21. ACID plot in T_1 at the UB3LYP/6-311+G(d,p) level of **DIAn-a**.

9.4 Cartesian coordinates

Supplementary Table 2. Cartesian coordinate of **DIAn-a** in singlet state optimized at RB3LYP/6-311G(d) level of theory.

atom	x	y	z
C	1.198133	0.785288	0.100175
C	2.377084	1.608252	0.198490
H	3.341749	1.114431	0.231178
C	2.274909	2.960386	0.247085
C	3.269581	4.026014	0.343470
C	4.655646	4.012597	0.424720
H	5.206309	3.076690	0.420415
C	5.340055	5.228112	0.514378
H	6.423301	5.231145	0.578123
C	4.643307	6.441923	0.524961
H	5.195506	7.373549	0.597842
C	3.251935	6.470616	0.445213
H	2.716862	7.414896	0.458185
C	2.556757	5.261053	0.351022
C	1.131548	4.989137	0.262524
C	0.968246	3.607671	0.200980
C	-0.193186	2.814132	0.099815
H	-1.166251	3.289455	0.057640
C	-0.106375	1.431300	0.050442
C	0.056982	6.012734	0.245491
C	-0.635760	6.323854	1.434364
C	-1.644837	7.290158	1.396094
H	-2.177079	7.537558	2.309971
C	-1.968011	7.940093	0.210239

C	-1.280041	7.630677	-0.957774
H	-1.532881	8.138062	-1.884217
C	-0.263850	6.671754	-0.960196
H	0.770590	5.698546	2.960723
H	-2.753408	8.689543	0.196981
Si	-5.256027	2.694990	-0.203814
C	-1.291355	0.604916	-0.051136
C	-2.561012	1.242307	-0.099653
C	-3.635816	1.811868	-0.140546
C	-6.631963	1.406348	-0.227186
H	-6.553065	0.750927	-1.099179
H	-6.605790	0.774995	0.665440
H	-7.616211	1.884197	-0.263328
C	-5.398866	3.788052	1.324331
H	-4.599901	4.533854	1.358170
H	-5.342161	3.200950	2.245068
H	-6.352819	4.325319	1.332541
C	-5.303314	3.741656	-1.769933
H	-6.254284	4.277794	-1.853243
H	-5.190202	3.127358	-2.667407
H	-4.502863	4.486529	-1.776940
C	-0.297732	5.636431	2.736790
H	-0.551688	4.572764	2.711625
H	-0.842289	6.087606	3.568716
C	0.461453	6.340971	-2.243447
H	0.069186	6.927300	-3.076752
H	0.359884	5.282812	-2.500593
H	1.533600	6.543136	-2.168014

C	-1.198133	-0.785288	-0.100175
C	-2.377084	-1.608252	-0.198490
H	-3.341749	-1.114431	-0.231178
C	-2.274909	-2.960386	-0.247085
C	-3.269581	-4.026014	-0.343470
C	-4.655646	-4.012597	-0.424720
H	-5.206309	-3.076690	-0.420415
C	-5.340055	-5.228112	-0.514378
H	-6.423301	-5.231145	-0.578123
C	-4.643307	-6.441923	-0.524961
H	-5.195506	-7.373549	-0.597842
C	-3.251935	-6.470616	-0.445213
H	-2.716862	-7.414896	-0.458185
C	-2.556757	-5.261053	-0.351022
C	-1.131548	-4.989137	-0.262524
C	-0.968246	-3.607671	-0.200980
C	0.193186	-2.814132	-0.099815
H	1.166251	-3.289455	-0.057640
C	0.106375	-1.431300	-0.050442
C	-0.056982	-6.012734	-0.245491
C	0.635760	-6.323854	-1.434364
C	1.644837	-7.290158	-1.396094
H	2.177079	-7.537558	-2.309971
C	1.968011	-7.940093	-0.210239
C	1.280041	-7.630677	0.957774
H	1.532881	-8.138062	1.884217
C	0.263850	-6.671754	0.960196
H	-0.770590	-5.698546	-2.960723

H	2.753408	-8.689543	-0.196981
Si	5.256027	-2.694990	0.203814
C	1.291355	-0.604916	0.051136
C	2.561012	-1.242307	0.099653
C	3.635816	-1.811868	0.140546
C	6.631963	-1.406348	0.227186
H	6.553065	-0.750927	1.099179
H	6.605790	-0.774995	-0.665440
H	7.616211	-1.884197	0.263328
C	5.398866	-3.788052	-1.324331
H	4.599901	-4.533854	-1.358170
H	5.342161	-3.200950	-2.245068
H	6.352819	-4.325319	-1.332541
C	5.303314	-3.741656	1.769933
H	6.254284	-4.277794	1.853243
H	5.190202	-3.127358	2.667407
H	4.502863	-4.486529	1.776940
C	0.297732	-5.636431	-2.736790
H	0.551688	-4.572764	-2.711625
H	0.842289	-6.087606	-3.568716
C	-0.461453	-6.340971	2.243447
H	-0.069186	-6.927300	3.076752
H	-0.359884	-5.282812	2.500593
H	-1.533600	-6.543136	2.168014

Supplementary Table 3. Cartesian coordinate of **DIAn-a** in triplet state optimized at UB3LYP/6-311G(d) level of theory.

atom	x	y	z
C	1.187148	0.789719	0.102820
C	2.361849	1.601956	0.203980
H	3.326376	1.108351	0.236612
C	2.260485	2.960699	0.255662
C	3.260242	4.022357	0.353298
C	4.645506	3.994070	0.433517
H	5.185207	3.051951	0.428596
C	5.345182	5.201520	0.522598
H	6.428396	5.190479	0.585559
C	4.664344	6.427364	0.533396
H	5.230317	7.350654	0.605505
C	3.276731	6.474817	0.454861
H	2.753222	7.425465	0.467480
C	2.560073	5.270773	0.361497
C	1.147694	5.027482	0.274414
C	0.962740	3.603899	0.209027
C	-0.184789	2.846335	0.106962
H	-1.158046	3.320326	0.064694
C	-0.104798	1.424408	0.052807
C	0.074128	6.049472	0.253596
C	-0.612806	6.369486	1.443556
C	-1.626462	7.330373	1.401605
H	-2.154795	7.584313	2.315927
C	-1.960266	7.965649	0.210576
C	-1.279224	7.646253	-0.958768
H	-1.541410	8.141485	-1.889162

C	-0.258932	6.691689	-0.957582
H	0.800310	5.820917	2.991997
H	-2.749858	8.710586	0.194117
Si	-5.261339	2.669733	-0.206679
C	-1.276177	0.624462	-0.049756
C	-2.548465	1.255040	-0.099423
C	-3.632264	1.808020	-0.141670
C	-6.622928	1.365168	-0.229739
H	-6.536099	0.710451	-1.101558
H	-6.589094	0.734448	0.663117
H	-7.612820	1.831260	-0.266045
C	-5.423290	3.763893	1.319425
H	-4.632955	4.518825	1.354946
H	-5.362385	3.178755	2.241176
H	-6.383386	4.290218	1.323954
C	-5.325973	3.716215	-1.772936
H	-6.283663	4.240597	-1.854629
H	-5.206625	3.103251	-2.670550
H	-4.534673	4.470865	-1.781701
C	-0.259005	5.697588	2.749621
H	-0.450569	4.621304	2.716209
H	-0.841624	6.113555	3.573957
C	0.460835	6.349708	-2.241113
H	0.043735	6.905016	-3.083529
H	0.385196	5.283447	-2.472547
H	1.527788	6.583360	-2.183066
C	-1.187148	-0.789719	-0.102820
C	-2.361849	-1.601956	-0.203980

H	-3.326376	-1.108351	-0.236612
C	-2.260485	-2.960699	-0.255662
C	-3.260242	-4.022357	-0.353298
C	-4.645506	-3.994070	-0.433517
H	-5.185207	-3.051951	-0.428596
C	-5.345182	-5.201520	-0.522598
H	-6.428396	-5.190479	-0.585559
C	-4.664344	-6.427364	-0.533396
H	-5.230317	-7.350654	-0.605505
C	-3.276731	-6.474817	-0.454861
H	-2.753222	-7.425465	-0.467480
C	-2.560073	-5.270773	-0.361497
C	-1.147694	-5.027482	-0.274414
C	-0.962740	-3.603899	-0.209027
C	0.184789	-2.846335	-0.106962
H	1.158046	-3.320326	-0.064694
C	0.104798	-1.424408	-0.052807
C	-0.074128	-6.049472	-0.253596
C	0.612806	-6.369486	-1.443556
C	1.626462	-7.330373	-1.401605
H	2.154795	-7.584313	-2.315927
C	1.960266	-7.965649	-0.210576
C	1.279224	-7.646253	0.958768
H	1.541410	-8.141485	1.889162
C	0.258932	-6.691689	0.957582
H	-0.800310	-5.820917	-2.991997
H	2.749858	-8.710586	-0.194117
Si	5.261339	-2.669733	0.206679

C	1.276177	-0.624462	0.049756
C	2.548465	-1.255040	0.099423
C	3.632264	-1.808020	0.141670
C	6.622928	-1.365168	0.229739
H	6.536099	-0.710451	1.101558
H	6.589094	-0.734448	-0.663117
H	7.612820	-1.831260	0.266045
C	5.423290	-3.763893	-1.319425
H	4.632955	-4.518825	-1.354946
H	5.362385	-3.178755	-2.241176
H	6.383386	-4.290218	-1.323954
C	5.325973	-3.716215	1.772936
H	6.283663	-4.240597	1.854629
H	5.206625	-3.103251	2.670550
H	4.534673	-4.470865	1.781701
C	0.259005	-5.697588	-2.749621
H	0.450569	-4.621304	-2.716209
H	0.841624	-6.113555	-3.573957
C	-0.460835	-6.349708	2.241113
H	-0.043735	-6.905016	3.083529
H	-0.385196	-5.283447	2.472547
H	-1.527788	-6.583360	2.183066

Supplementary Table 4. Cartesian coordinate of **DIAn-b** in singlet state optimized at RB3LYP/6-311G(d) level of theory.

atom	x	y	z
C	0.552243	-1.319486	0.000000
C	1.069783	-2.664222	0.000000
H	2.148193	-2.800254	0.000000
C	0.223550	-3.725300	0.000000
C	0.444850	-5.169052	0.000000
C	1.599611	-5.941625	0.000000
H	2.582204	-5.479005	0.000000
C	1.483085	-7.333470	0.000000
H	2.377745	-7.947491	0.000000
C	0.223550	-7.946411	0.000000
H	0.157896	-9.029836	0.000000
C	-0.942752	-7.186067	0.000000
H	-1.914368	-7.670719	0.000000
C	-0.841208	-5.790297	0.000000
C	-1.851093	-4.761448	0.000000
C	-1.230033	-3.522781	0.000000
C	-1.748221	-2.209383	0.000000
H	-2.823251	-2.049984	0.000000
C	-0.894866	-1.116434	0.000000
H	-2.919995	-4.937017	0.000000
C	-1.382934	0.222900	0.000000
H	-2.459683	0.374100	0.000000
C	-0.552243	1.319486	0.000000
C	-1.069783	2.664222	0.000000
H	-2.148193	2.800254	0.000000
C	-0.223550	3.725300	0.000000

C	-0.444850	5.169052	0.000000
C	-1.599611	5.941625	0.000000
H	-2.582204	5.479005	0.000000
C	-1.483085	7.333470	0.000000
H	-2.377745	7.947491	0.000000
C	-0.223550	7.946411	0.000000
H	-0.157896	9.029836	0.000000
C	0.942752	7.186067	0.000000
H	1.914368	7.670719	0.000000
C	0.841208	5.790297	0.000000
C	1.851093	4.761448	0.000000
C	1.230033	3.522781	0.000000
C	1.748221	2.209383	0.000000
H	2.823251	2.049984	0.000000
C	0.894866	1.116434	0.000000
H	2.919995	4.937017	0.000000
C	1.382934	-0.222900	0.000000
H	2.459683	-0.374100	0.000000

Supplementary Table 5. Cartesian coordinate of **DIAn-b** in triplet state optimized at UB3LYP/6-311G(d) level of theory.

atom	x	y	z
C	0.547957	-1.312926	0.000000
C	1.073905	-2.646148	0.000000
H	2.152700	-2.777290	0.000000
C	0.231037	-3.717357	0.000000
C	0.468982	-5.160452	0.000000
C	1.635012	-5.912927	0.000000
H	2.609319	-5.433394	0.000000
C	1.543738	-7.308303	0.000000
H	2.449934	-7.905145	0.000000
C	0.295052	-7.947378	0.000000
H	0.251686	-9.031832	0.000000
C	-0.883348	-7.210944	0.000000
H	-1.846210	-7.712595	0.000000
C	-0.810297	-5.807712	0.000000
C	-1.831653	-4.813458	0.000000
C	-1.213544	-3.525831	0.000000
C	-1.746237	-2.253451	0.000000
H	-2.821527	-2.098649	0.000000
C	-0.883348	-1.116050	0.000000
H	-2.897884	-5.001559	0.000000
C	-1.383622	0.192382	0.000000
H	-2.460443	0.340932	0.000000
C	-0.547957	1.312926	0.000000
C	-1.073905	2.646148	0.000000
H	-2.152700	2.777290	0.000000
C	-0.231037	3.717357	0.000000

C	-0.468982	5.160452	0.000000
C	-1.635012	5.912927	0.000000
H	-2.609319	5.433394	0.000000
C	-1.543738	7.308303	0.000000
H	-2.449934	7.905145	0.000000
C	-0.295052	7.947378	0.000000
H	-0.251686	9.031832	0.000000
C	0.883348	7.210944	0.000000
H	1.846210	7.712595	0.000000
C	0.810297	5.807712	0.000000
C	1.831653	4.813458	0.000000
C	1.213544	3.525831	0.000000
C	1.746237	2.253451	0.000000
H	2.821527	2.098649	0.000000
C	0.883348	1.116050	0.000000
H	2.897884	5.001559	0.000000
C	1.383622	-0.192382	0.000000
H	2.460443	-0.340932	0.000000

10. OFET device data

10.1 Transistor Fabrication and Characterization.

Field-effect transistors were fabricated by vapour deposition of ~50 nm thick layers of the semiconductors at preselected temperatures (~6 x 10^{-6} torr, 0.2 Å s^{-1}) on p-doped Si (001) wafers with a 300 nm thermally grown SiO_2 dielectric layer. The SiO_2 substrate was heated at 150 °C and the DIAn source was heated 160–201 °C. Prior to deposition, the wafers were cleaned by rinsing twice with EtOH followed by a 5 min plasma cleaning in a Harrick PDC-32G Plasma Cleaner/Sterilizer. A self-assembled monolayer (SAM) of either hexamethyldisilazane (HMDS) or octadecyltrichlorosilane (OTS) was then deposited to reduce charge trapping and thus enhance mobility. Treatment with HMDS was carried out by exposing the cleaned silicon wafers to HMDS vapour at room temperature in a closed air-free container under argon, whereas treatment with OTS was performed by immersing the silicon wafers in a 3.0 mM humidity-exposed OTS-hexane solution for 1 hour, as previously described.

Solution-processed OFETs were fabricated either by spin-coating of a 7 mg ml^{-1} solution in $CHCl_3$ or by drop-casting of a 5 mg ml^{-1} solution in $CHCl_3$. Due to the hydrophobicity of the substrates, spreading of the solutions with the tip of the pipette helped to achieve a homogenous deposition.

Top contact OFETs were fabricated by vapour deposition of Au electrodes (~10^{-7} torr, 0.2 Å s^{-1}, ~50 nm thick) onto the semiconductor thin films through a shadow mask to obtain devices with deliberately varied channel widths and lengths. The capacitance of the 300 nm SiO_2 gate insulator is 1 x 10^{-8} F cm^{-2}. Characterization of the devices was performed under vacuum in a customized high-vacuum probe station (~10^{-6} torr) and in ambient atmosphere using an EB-4 Everbeing probe station with a 4200-SCS/C Keithley semiconductor characterization system.

Supplementary Table 6 shows the electrical performance parameters of OFETs fabricated by vapour-deposition of the semiconductor. The corresponding output I-V$_{SD}$ plots are shown in Supplementary Figure 22. Note that performances of devices with no SAM treatment or treated with HMDS are only modest. Recently, it has been found a similar behavior for a biradical organic semiconductor, where HMDS treatment rendered non-active devices, whereas trichlorosilane-derived SAM-treated devices showed ambipolar characteristics.[24] On the contrary, devices fabricated using OTS-treated gate dielectrics give ambipolar performances with

quite balanced electron and hole mobilities (Supplementary Table 6). During vapour-deposition the substrates were preheated at different temperatures in order to improve film morphology and crystallinity. Analysis of these devices indicates a gradual increase of electron mobility with temperature at the expense of the hole mobility. Nevertheless, mobilities in the range of $10^{-3} - 10^{-2}$ cm^2 V^{-1} s^{-1} are registered for the whole temperature range analyzed. These values are comparable with previously reported for organic biradicals.[24,25] It should be noted that under ambient conditions, **DIAn** behaves solely as a p-type semiconductor, with mobilities as high as 4.5×10^{-2} cm^2 V^{-1} s^{-1}.

Supplementary Table 6. OFET electrical data for vapour-deposited films of the material deposited on untreated, HMDS-treated and OTS-treated gate dielectrics. Measurements were carried out in vacuum and in ambient conditions.

		Vaccuum						Air		
		μ_h [cm^{2}V^{-1}s^{-1}]	V_T [V]	Ion/Ioff	μ_e [cm^{2}V^{-1}s^{-1}]	V_T [V]	Ion/Ioff	μ_h [cm^{2}V^{-1}s^{-1}]	V_T [V]	Ion/Ioff
OTS	150	2,28E-03	22	5,E+00	3,97E-03	32	5,E+00	2,18E-02	-4	2,E+04
	100	5,19E-03	18	3,E+00	1,22E-03	76	2,E+00	4,53E-02	-2	5,E+04
	Tamb	7,41E-03	8	1,E+01	1,78E-03	27	4,E+00	3,09E-05	10	1,E+04
HMDS	150	1,41E-05	15	6,E+00				5,27E-05	-16	4,E+03
	Tamb	3,64E-06	28	3,E+00				8,20E-05	-3	7,E+03
Sintto	150	1,10E-05	-11	2,E+03				1,29E-05	-53	4,E+02
	100	1,21E-03	-15	6,E+02				4,06E-05	5	6,E+03
	Tamb	2,68E-04	-18	8,E+02				4,38E-05	3	1,E+03
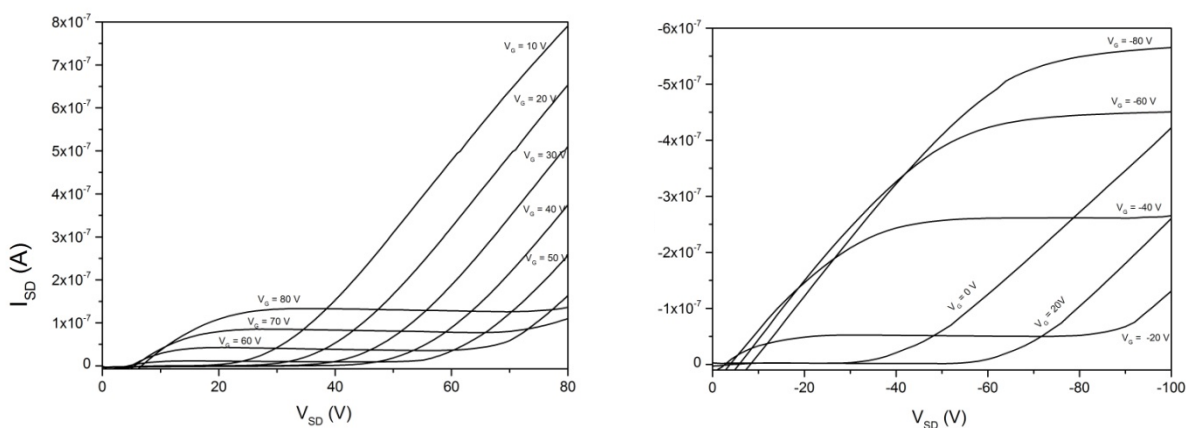
Supplementary Figure 22. Selected output plot data for vapour-deposited films grown on OTS-treated Si/SiO$_2$ substrates: (left) Electron-transport characteristics for films deposited on substrates pre-heated at 150 ºC. (right) Hole-transport characteristics for films deposited at 25 ºC.

Supplementary Table 7 shows the electrical performances of solution-processed films. Under these conditions the semiconductor only behaves as a p-type material both under vacuum or ambient environments, showing similar field-effect mobilities to the vapour-deposited devices. Additional improvements are underway to optimize these conditions.

Supplementary Table 7. OFET electrical data for solution-processed films of the material deposited on HMDS-treated and OTS-treated gate dielectrics. Measurements were carried out in vacuum and in ambient conditions.

		Vaccuum			Air		
		μ_h [cm^{2}V^{-1}s^{-1}]	V_T [V]	Ion/Ioff	μ_h [cm^{2}V^{-1}s^{-1}]	V_T [V]	Ion/Ioff
OTS [a]	100	3,38E-03	-11	5,45E+02	3,32E-03	-19	4,40E+04
	Tamb	1,27E-03	-6	7,53E+02	2,19E-03	-18	4,28E+04
HMDS [b]	Tamb	3,18E-06	-20	8,46E+01	2,46E-06	16	3,41E+02

[a]: spin-coating
[b]: drop-casting

11. Supplementary references

1. Park, J.-H.; Chung, D. S.; Park, J. W.; Ahn, T.; Kong, H.; Jung, Y. K.; Lee, J.; Yi, M. H.; Park, C. E.; Kwon, S.-K.; Shim, H-K. *Org. Lett.* **2007**, *9*, 2573–2576.

2. Reiss, H.; Heller, A. *J. Phys. Chem.* **1985**, *89*, 4207–4213.

3. Sheldrick, G. M. *Bruker/Siemens Area Detector Absorption Correction Program*, Bruker AXS, Madison, WI, 1998.

4. Sheldrick, G. M. *Acta Cryst.* **2008**, *A64*, 112–122.

5. Bleaney, B.; Bowers, K. D. *Proc. R. Soc. Lond. A.* **1952**, *214*, 451–465.

6. Gaussian 09, Revision A.02, Frisch, M. J.; Trucks, G. W.; Schlegel, H. B.; Scuseria, G. E.; Robb, M. A.; Cheeseman, J. R.; Scalmani, G.; Barone, V.; Mennucci, B.; Petersson, G. A.; Nakatsuji, H.; Caricato, M.; Li, X.; Hratchian, H. P.; Izmaylov, A. F.; Bloino, J.; Zheng, G.; Sonnenberg, J. L.; Hada, M.; Ehara, M.; Toyota, K.; Fukuda, R.; Hasegawa, J.; Ishida, M.; Nakajima, T.; Honda, Y.; Kitao, O.; Nakai, H.; Vreven, T.; Montgomery, Jr., J. A.; Peralta, J. E.; Ogliaro, F.; Bearpark, M.;. Heyd, J. J; Brothers, E.; Kudin, K. N.; Staroverov, V. N.; Kobayashi, R.; Normand, J.; Raghavachari, K.; Rendell, A.; Burant, J. C.; Iyengar, S. S.; Tomasi, J.; Cossi, M.; Rega, N.; Millam, J. M.; Klene, M.; Knox, J. E.; Cross, J. B.; Bakken, V.; Adamo, C.; Jaramillo, J.; Gomperts, R.; Stratmann, R. E.; Yazyev, O.; Austin, A. J.; Cammi, R.; Pomelli, C.; Ochterski, J. W.; Martin, R. L.; Morokuma, K.; Zakrzewski, V. G.; Voth, G. A.; Salvador, P.; Dannenberg, J. J.; Dapprich, S.; Daniels, A. D.; Farkas, O.; Foresman, J. B.; Ortiz, J. V.; Cioslowski, J.; Fox, D. J.; Gaussian, Inc., Wallingford CT, 2009.

7. Schmidt, M. W.; Baldridge, K. K.; Boatz, J. A.; Elbert, S. T.; Gordon, M. S.; Jensen, J. H.; Koseki, S.; Matsunaga, H.; Nguyen, K. A.; Su, S.; Windus, T. L.; Dupuis, M.; Montgomery, Jr. J. A. *J. Comput. Chem.* **2003**, *14*, 1347–1363.

8. Shao, Y.; Fusti-Molnar, L.; Jung, Y.; Kussmann, J.; Ochsenfeld, C.; Brown, S. T.; Gilbert, A. T. B.; Slipchenko, L. V.; Levchenko, S. V.; O'Neill, D. P. et. al. Q-CHEM, version 4.1; Q-Chem. Inc.: Pittsburgh, PA, 2008.

9. Shao, Y.; Head-Gordon, M.; Krylov, A. I. *J. Chem. Phys.* **2003**, *118*, 4807–4818.

10. Y. A. Bernard, Y. Shao and A. I. Krylov. *J. Chem. Phys.* **2012**, *136*, 204103–1–17.

11. Fukui, H.; Nakano, M.; Shigeta, Y.; Champagne, B. *J. Phys. Chem. Lett.* **2011**, *2*, 2063–2066.

12. (a) Head-Gordon, M. *Chem. Phys. Lett.* **2003**, *372*, 508-511. (b) Nakano, M.; Fukui, H.; Minami, T.; Yoneda, K.; Shigeta, Y.; Kishi, R.; Champagne, B.; Botek, E.; Kubo, T.; Ohta, K.; Kamada, K. *Theoret. Chem. Acc.* **2011**, *130*, 711-724; *erratum* **2011**, *130*, 725. (c) Takatsuka, K.; Fueno, T.; Yamaguchi, K. *Theoret. Chim. Acta (Berl.)* **1978**, *48*, 175-183.

13. Gershoni-Poranne, R.; Stanger, A. *Chem. Eur. J.* **2014**, *20*, 5673–5688.

14. Rahalkar, A.; Stanger, A. "Aroma", http://schulich.technion.ac.il/Amnon_Stanger.htm

15. Stephens, P. J.; Devlin, F. J.; Chabalowski, C. F.; Frisch M. J. *J. Phys. Chem.* **1994**, *98*, 11623–11627.

16. (a) Becke, A. D. *Phys. Rev. A* **1988**, *38*, 3098–3100. (b) Lee, C.; Yang, W.; Parr, R. G. *Phys. Rev. B* **1988**, *37*, 785–789.

17. Iikura, H.; Tsuneda, T.; Yanai, T.; Hirao, K. *J. Chem. Phys.* **2001**, *115*, 3540–3544.

18. Krishnan, R.; Binkley, J. S.; Seeger, R.; Pople, J. A. *J. Chem. Phys.* **1980**, *72*, 650–654.

19. Wolinski, K.; Hinton, J. F.; Pulay, P. *J. Am. Chem. Soc.* **1990**, *112*, 8251–8260.

20. Stanger, A. *J. Org. Chem.* **2010**, *75*, 2281–2288.

21. (a) Herges, R.; Geuenich, D. *J. Phys. Chem. A* **2001**, *105*, 3214–3220. (b) Geuenich, D.; Hess, K.; Kohler, F.; Herges, R. *Chem. Rev.* **2005**, *105*, 3758–3772.

22. Keith, T. A.; Bader, R. F. W. *Chem. Phys. Lett.* **1993**, *210*, 223–231.

23. Kishi, R.; Bonness, S.; Yoneda, K.; Takahashi, H.; Nakano, M.; Botek, E.; Champagne, B.; Kubo, T.; Kamada, K.; Ohta, K.; Tsuneda, T. *J. Chem. Phys.* **2010**, *132*, 094107-1-11.

24. Koike, H.; Chikamatsu, M.; Azumi, R.; Tsutsumi, J. y.; Ogawa, K.; Yamane, W.; Nishiuchi, T.; Kubo, T.; Hasegawa, T.; Kanai, K. *Adv. Funct. Mater.* **2015**, *26*, 277–283.

25. Chikamatsu, M.; Mikami, T.; Chisaka, J.; Yoshida, Y.; Azumi, R.; Yase, K.; Shimizu, A.; Kubo, T.; Morita, Y.; Nakasuji, K. *Appl. Phys. Lett.* **2007**, *91*, 043506-1–043506-3.